R-804 DECEMBER, 1977 UILU-ENG 77-2251

CSL COORDINATED SCIENCE LABORATORY

ACCURACY TESTS FOR ASYMPTOTIC SOLUTIONS TO RADIATION FROM A CYLINDER

M. TEW
R. MITTRA

UNIVERSITY OF ILLINOIS - URBANA, ILLINOIS

REPORT DOCUMENTATION PAGE

READ INSTRUCTIONS BEFORE COMPLETING FORM

1. REPORT NUMBER	2. GOVT ACCESSION NO. / 3. RECIPIENT'S CATALOG NUMBER
4. TITLE (and Subtitle): ACCURACY TESTS FOR ASYMPTOTIC SOLUTIONS TO RADIATION FROM A CYLINDER	5. TYPE OF REPORT & PERIOD COVERED: Technical Report
	6. PERFORMING ORG. REPORT NUMBER: R-804; UILU-ENG 77-2251
7. AUTHOR(s): M. Tew and R. Mittra	8. CONTRACT OR GRANT NUMBER(s): DAAB-07-72-C-0259; N000 19-77-C-9127
9. PERFORMING ORGANIZATION NAME AND ADDRESS: Coordinated Science Laboratory, University of Illinois at Urbana-Champaign, Urbana, Illinois 61801	10. PROGRAM ELEMENT, PROJECT, TASK AREA & WORK UNIT NUMBERS
11. CONTROLLING OFFICE NAME AND ADDRESS: Joint Services Electronics Program	12. REPORT DATE: December, 1977
	13. NUMBER OF PAGES: 55
14. MONITORING AGENCY NAME & ADDRESS (if different from Controlling Office)	15. SECURITY CLASS. (of this report): UNCLASSIFIED
	15a. DECLASSIFICATION/DOWNGRADING SCHEDULE

16. DISTRIBUTION STATEMENT (of this Report)

Approved for public release; distribution unlimited

17. DISTRIBUTION STATEMENT (of the abstract entered in Block 20, if different from Report)

18. SUPPLEMENTARY NOTES

19. KEY WORDS (Continue on reverse side if necessary and identify by block number)

Electromagnetic Radiation and Scattering
Asymptotic Solutions
Accuracy Tests
Geometrical Theory of Diffraction

20. ABSTRACT (Continue on reverse side if necessary and identify by block number)

The problem of determining the induced surface currents on an infinite circular cylinder excited by a slot radiator has received increased attention in recent years. One reason for this interest is the usefulness of the induced currents in calculating various electrical parameters. In a conformal slot array, for instance, knowledge of the currents allows calculation of both the mutual impedance between two slots and the far-field pattern. The work reported here is concerned with tests which attempt to evaluate the accuracy of existing solutions for the infinite cylinder problem.

UILU-ENG 77-2251

ACCURACY TESTS FOR ASYMPTOTIC SOLUTIONS TO RADIATION FROM A CYLINDER

by

M. Tew and R. Mittra

This work was supported in part by the Joint Services Electronics Program (U.S. Army, U.S. Navy and U.S. Air Force) under Contract DAAB-07-72-C-0259 and in part by the Naval Air System under Grant N000 19-77-C-9127.

TABLE OF CONTENTS

LIST OF FIGURES

LIST OF TABLES

1.0 Introduction

The problem of determining the induced surface currents on an infinite circular cylinder excited by a slot radiator has received increased attention in recent years. One reason for this interest is the usefulness of the induced currents in calculating various electrical parameters. In a conformal slot array, for instance, knowledge of the currents allows calculation of both the mutual impedance between two slots and the far-field pattern. The work reported here is concerned with tests which attempt to evaluate the accuracy of existing solutions for the infinite cylinder problem.

An exact modal solution to the cylinder problem does exist [1]-[2]. However, for large radii the solution (whose form is an infinite series with each term containing an infinite integral) converges so slowly as to make its use impractical. For large kR (k the wavenumber and R the radius), three asymptotic solutions have been published [3]-[7]. Two of the asymptotic solutions are derived from manipulation of the modal solution (hereafter referred to as the OSU [3]-[4] and PINY [5]-[6] solutions), while the third is based on the work of V. A. Fock addressing the problem of radiation on a sphere (the UI solution [7]).

Because all of the asymptotic solutions for the cylinder are approximate, a test which could determine the relative accuracy of the solution is highly desirable. If the test also gave information about the local accuracy (i.e. provided information about the source region accuracy, accuracy for large path lengths, etc.), it would be even more valuable. This report proposes two such tests: one based on satisfaction of the E-field boundary condition and one based on

Lorentz reciprocity. The tests are applied to the OSU solution, a modified version of the OSU solution, and to the UI solution. When possible, an exact analytic solution was also tested.

1.1 The Problem

The problem addressed consists of an infinite, perfectly conducting cylinder of radius R as shown in Figure 1a. A standard ρ, ϕ, z cylindrical coordinate system is imposed on the cylinder so that the z-axis coincides with the cylinder axis. The coordinate system is set up so that $\rho=R$, $\phi=0$, $z=0$ defines the center of the slot (or coincides with an elemental magnetic dipole radiator). As shown, s is the path length on the cylinder surface and θ is measured from the ϕ-axis to the surface path.

The cylinder is a developable surface, and a geodesic path on the cylinder surface becomes a straight line on the infinite strip that makes up a developed cylinder. Figure 1b shows the developed cylinder and introduces the local $\hat{n}',\hat{b}',\hat{t}'$ and $\hat{n},\hat{b},\hat{t}$ coordinate systems, where $\hat{n}',\hat{n}$ are the outward normal to the surface and $\hat{t}',\hat{t}$ are tangent to the surface path at the source and observation points, respectively ($\hat{b}'=\hat{t}' \times \hat{n}'$, $\hat{b}=\hat{t} \times \hat{n}$). On the developed cylinder $\hat{t}'$ is parallel to $\hat{t}$, $\hat{n}'$ is parallel to $\hat{n}$, and $\hat{b}'$ is parallel to $\hat{b}$; however, this is not the case for the undeveloped cylinder (figure 1c). Each of the asymptotic solutions tested determines the surface H-field components at the observation point, Q, in terms of the field parallel to the surface ray, H_t, and the field perpendicular to both the surface ray and the surface normal, H_b. Thus, each solution tested is of the form

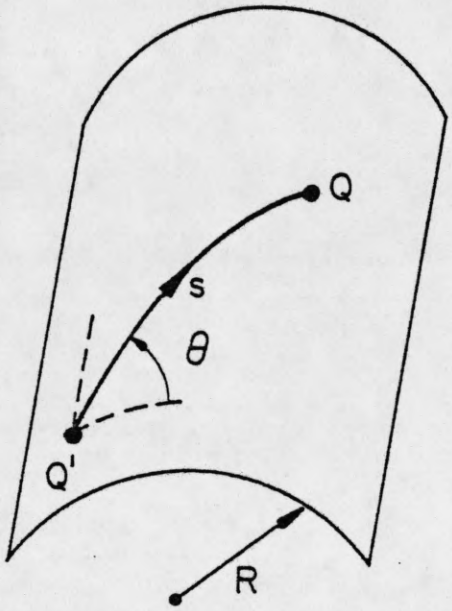

(a) 3-D view

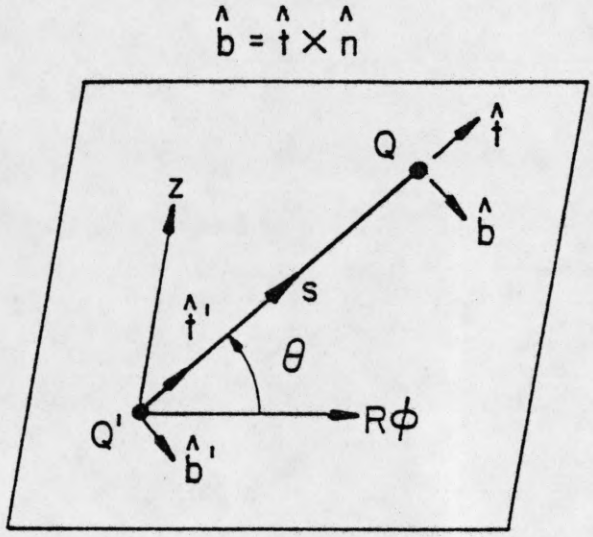

(b) Developed cylinder

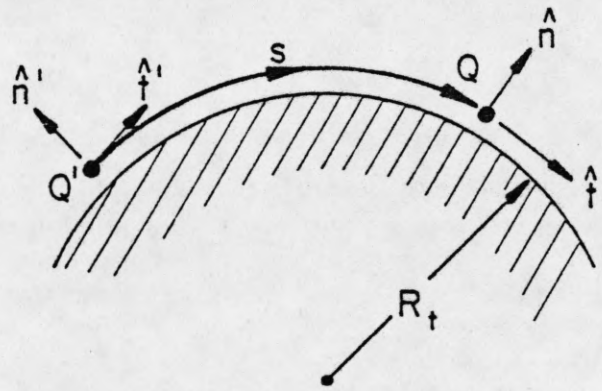

(c) Cut along θ-direction

A surface ray from source point Q' to observation point Q on a cylinder of radius R.

Fig. 1. Problem Geometry

$$\bar{H}(Q) = \bar{M} \cdot (\hat{b}'\hat{b}\, H_b + \hat{t}'\hat{t}\, H_t)$$

where $\bar{M}$ is the magnetic dipole moment. For all results reported here, $\bar{M} = \hat{\phi}$, i.e., a circumferentially oriented source was used.

1.2 Solutions Tested

The results of tests on three asymptotic solutions are included : the OSU solution, the UI solution, and a modified version of the OSU solution.

The OSU solution is given by

$$H_b(Q) \sim v(\xi)\, G(s) \qquad \text{(Eq. 1.2-1)}$$

$$H_t(Q) \sim (2j/ks)\, u(\xi)\, G(s)$$

$$\eta = \sqrt{\frac{\mu_o}{\varepsilon_o}} \simeq 377\ \Omega \quad ; \quad \xi = \left(\frac{k}{2 R_t^2}\right)^{1/3} s.$$

$$G(s) = \frac{k^2}{2\pi j \eta}\ \frac{e^{-jks}}{ks}$$

where η is the impedance of free space, and u and v are Fock functions. ξ is a normalized distance parameter, with R_t being the radius of curvature along the surface ray path (radius of curvature in the direction of $\hat{t}$). For the cylinder case under consideration, $R_t = R/\cos^2\theta$. Note that $\xi \to 0$ whenever $R \to \infty$ or $\theta \to \pi/2$. For the case when $\xi \to 0$ the OSU solution reduces to

$$H_b(Q) \sim G(s) \qquad \text{(Eq. 1.2-2)}$$

$H_t(Q) \sim (2j/ks)\, G(s)$ and the form of H_b recovers identically the $(ks)^{-1}$ term from the exact solution of a magnetic dipole radiating on an infinite flat ground plane.

The UI solution is found by (Eq. 1.2-3)

$$H_b(Q) \sim [(1-j/ks)\, v(\xi) - (1/ks)^2\ u(\xi) + j(\sqrt{2}\, kR_t)^{-2/3}\, v'(\xi) + j(\sqrt{2}\, kR_t)^{-2/3}$$

$$(R_t/R_b)\ u'(\xi)]\, G(s)$$

$$H_t(Q) \sim (j/ks)\, [v(\xi) + (1-2j/ks)\ u(\xi) + j(\sqrt{2}\, kR_t)^{-2/3}\ u'(\xi)]\, G(s)$$

where v,u are Fock functions, v' and u' are their derivatives, respectively. ξ and G(s) were defined above, and R_b is the radius of curvature transverse to the surface ray (radius of curvature in the direction of $\hat{b}$). Two features of the UI solution stand out. As $kR \to \infty$ the solution reduces to

$$H_b(Q) \sim [1-j/ks-(1/ks)^2]\, G(s) \qquad \text{(Eq. 1.2-4)}$$

$$H_t(Q) \sim (2j/ks)\, [1-j/ks]\, G(s)$$

which identically recovers the exact solution for a magnetic dipole radiating on an infinite flat plane (this is in contrast to the OSU solution which recovered only the 1/s term of H_b and the $1/s^2$ term of H_t). As $\theta \to \pi/2$ the UI solution may be put in the following form:

$$H_b(Q) \sim [\, H_b(Q)\,]_{PLANAR} + (A/kR)\, e^{-jks}/\sqrt{ks} \qquad \text{(Eq. 1.2-5)}$$

where A is a constant. The surface ray along the cylinder axis thus exhibits less attenuation than a corresponding ray on a flat plane. (This type of asymptotic behaviour as $\theta \to \pi/2$ is also exhibited by the PINY solution).

Thus, two distinct differences exist between the OSU and UI solutions in the limiting cases of $kR \to \infty$ and $\theta \to \pi/2$. One concerns the higher-order terms ($1/s^2$, $1/s^3$) of the solution and may be thought

of as a localized, source-region effect. The other difference lies in the attenuation of a ray propagating along the cylinder axis ($\theta = \pi/2$) where the OSU solution decays as $1/s$ and the UI solution decays as $1/\sqrt{s}$. This effect, then, is hardly significant near the source, where the $1/s^2$ and $1/s^3$ terms dominate, but determines the field behaviour far away from the source.

In order to attempt to separate the above two effects, a third solution has been constructed, called the modified OSU solution (OSUMOD). The OSUMOD solution is given by

$$H_b(Q) \sim [\, v(\xi) - j/ks - (1/ks)^2 \,]\, G(s) \qquad \text{(Eq. 1.2-6)}$$

$$H_t(Q) \sim (2j/ks)\, [\, u(\xi) - j/ks \,]\, G(s)$$

As is apparent, the OSU solution has been modified by the addition of the higher-order terms present in the exact solution of the planar problem. The OSUMOD solution will recover the exact planar solution when $kR \to \infty$, just as the UI solution does. However, along $\theta = \pi/2$ the OSUMOD solution decays as $1/s$, while the UI solution decays as $1/\sqrt{s}$.

The rationale behind creation of the OSUMOD solution is contained in the following argument:

The OSU and UI solutions are quite different - - not only in the construction of the solution, but also in the behaviour under limiting cases. Both the source region behaviour and the "asymptotic" behaviour (for large ks along $\theta = \pi/2$) are significantly different. Even if a test revealed differences between the UI and OSU solutions, it might still be difficult to determine the local accuracy of the solution, i.e. it might be difficult to determine the

"cause" of the difference in test results. Creation of the OSUMOD solution is designed to alleviate this problem. Since OSU and OSUMOD have the same behaviour as $\theta \to \pi/2$, comparison of their test results may reveal the role of the source region in satisfaction of the test. Similarly, OSUMOD and UI have the same behaviour in the source region (as $kR \to \infty$), so comparison of their test results may reveal the role of the $1/\sqrt{s}$ term.

In review, we have three asymptotic solutions to test - - two have been published, and the third has been created to somewhat bridge the differences between the first two. Two tests are proposed:

1) Test for satisfaction of the E-field boundary condition on the cylinder surface,and

2) Test for satisfaction of Lorentz reciprocity.

2.0 E-field Test

The tangential E-field must be zero everywhere on the surface of a perfect conductor. The exact solution for a circumferential slot radiating on a perfectly conducting circular cylinder thus would have $E_\phi=0$ everywhere on the cylinder and $E_z=0$ everywhere except in the extent of the slot. The E-field test checks to see how well the asymptotic solutions satisfy this condition.

The E-field test is conducted in the following manner: Each of the asymptotic solutions predicts the H-field on the cylinder surface. Through the use of Maxwell's equations the surface H-field may be related to the surface E-field and the boundary condition checked. Use of the spectrum of the H-field instead of the direct surface field

makes analysis straightforward and allows use of a Fast-Fourier Transform (FFT) algorithm for efficient numerical calculation.

The test proceeds as follows:

1) A cylindrical transform is defined

$$\underset{\phi}{\tilde{H}_z}(n,k_z) = 1/2\pi \int_0^{2\pi} d\phi \int_{-\infty}^{\infty} dz \; \underset{\phi}{H_z}(\phi,z)\; e^{-jn\phi}\; e^{-jk_z z} \qquad \text{(Eq.2.0-1)}$$

2) Electric and magnetic vector potentials are expanded with unknown coefficients (Eq. 2.0-2)

$$\begin{pmatrix} A_z \\ F_z \end{pmatrix} = \frac{1}{2\pi} \sum_{n=-\infty}^{\infty} e^{jn\phi} \int_{-\infty}^{\infty} \begin{pmatrix} f_n(k_z) \\ g_n(k_z) \end{pmatrix} H_n^{(2)}(\rho\sqrt{k^2-k_z^2})\; e^{jk_z z}\, dz$$

Observe that n and k_z are "transform variables," k is the wavenumber, and $H_n^{(2)}$ is the n^{th} order Hankel function of the second kind, representing an outward-traveling cylindrical wave. For future notation, the complex variable γ will be used to replace the radical in the argument of the Hankel function, $\gamma = \sqrt{k^2-k_z^2}$.

3) Through the use of

$$\overline{H} = \nabla x \overline{A} - j\omega\varepsilon_o \overline{F} + 1/j\omega\mu_o \; \nabla\nabla\cdot\overline{F} \qquad \text{(Eq.2.0-3)}$$

one may determine the unknown coefficients f_n and g_n in terms of the transform of the surface H-field as (Eq.2.0-4)

$$f_n(k_z) = \frac{-1}{\gamma H_n'^{\,2}(\gamma R)} \left[\tilde{H}_\phi(n,k_z) + \frac{n\,k_z}{\gamma^2 R}\; \tilde{H}_z(n,k_z)\right]$$

$$g_n(k_z) = \frac{jw\,\mu_o}{\gamma^2 H_n^{\,2}(\gamma R)}\; \tilde{H}_z(n,k_z)$$

where $H_n'^{(2)}$ is the derivative of the $H_n^{(2)}$ Hankel function.

4) Applying

$$\overline{E} = -\nabla x\overline{F} - j\omega\mu_o\overline{A} + 1/j\omega\varepsilon_o\ \nabla\nabla\cdot\overline{A} \qquad \text{(Eq.2.0-5)}$$

permits computation of the surface E-field, accomplishing the desired test.

The preceding procedure can be compressed into two steps of actual computation:

1) Compute the spectrum of the surface H-field from Equation 2.0-1, then

2) Compute the surface E-field from (Eq. 2.0-6)

$$E_z(a, \phi, z) = \frac{1}{2\pi} \sum_{n=-\infty}^{\infty} e^{jn\phi} \int_{-\infty}^{\infty} dk_z$$

$$\{ \left(\frac{-\gamma}{j\omega\varepsilon_o}\right) \left(\frac{H_n^2(\gamma R)}{H_n'^2(\gamma R)}\right) \left(\tilde{H}_\phi(n,kz) + \frac{n\,k_z}{\gamma^2 R} \tilde{H}_z(n,k_z)\right)\} \ e^{jk_z z}$$

$$E_\phi(a, \phi, z) = \frac{1}{2\pi} \sum_{n=-\infty}^{\infty} e^{jn\phi} \int_{-\infty}^{\infty} dk_z \left\{ \frac{n\,k_z}{j\omega\varepsilon_o\gamma R} \frac{H_n^2(\gamma R)}{H_n'^2(\gamma R)} \tilde{H}_\phi(n,k_z)\right.$$

$$\left. + \tilde{H}_z(n,k_z) \left[\frac{j\omega\mu_o}{\gamma} \frac{H_n'^2(\gamma R)}{H_n^2(\gamma R)} + \frac{(nk_z)^2}{j\omega\varepsilon_o\gamma^3 R^2} \frac{H_n^2(\gamma R)}{H_n'^2(\gamma R)}\right] \right\} e^{jk_z z}$$

The above two-step procedure is significant because, while the expressions appear to be complex, they essentially involve only a two-dimensional Fourier transform, modification and combination of the transformed fields, and then inverse Fourier transformation and summation of Fourier coefficients. The analysis is computationally efficient because the FFT can be used to evaluate all the integrals involved.

Practically speaking, the greatest difficulty in the above procedure comes in trying to get an accurate assessment of the spectrum of the surface H_ϕ field. Both the OSUMOD and UI solutions have singularities on the order of $1/s^2$ and $1/s^3$, while the OSU solution has a singularity on the order of $1/s$. The "peakiness" of these H_ϕ fields means that special care must be taken in using the FFT to determine the spectrum.

The first attempt to overcome this problem involved raising the magnetic dipole slightly above the cylinder surface so that the field was no longer singular, but had a finite peak. After this step had been implemented, a convergence check of the FFT integral showed that the FFT was able to handle the $1/s$ peak correctly with reasonable sampling rates, but the $1/s^2$ and $1/s^3$ peaks yielded erroneous results. Further measures were necessary to achieve a reliable test of the OSUMOD and UI solutions (for a reasonable computer size).

The key to achieving a reliable check of the UI and OSUMOD solutions lies in recognizing that the singular form of the source region is that of a planar case, and that the singularity has an analytic transform. Specifically, the planar singularity can be expressed as (Eq. 2.0-7)

$$H_\phi\Big|_s = \frac{1}{2\pi\eta jk}\left(\frac{\partial^2}{\partial(R\phi)^2} + k^2\right)\frac{e^{-jks}}{s}$$

$$H_z\Big|_s = \frac{1}{2\pi\eta jk}\left(\frac{\partial^2}{\partial(R\phi)\partial z}\right)\frac{e^{-jks}}{s}$$

where s is the path length given by $s = \sqrt{\Delta^2+(R\phi)^2+z^2}$, and Δ is the height of the dipole above the cylinder. Because the singularities

may be expressed as derivatives, their analytic transform is obtainable and is of the form (Eq.2.0-8)

$$\tilde{H}_z\Big|_s = \frac{Q}{2\Pi\eta jk}\left(\frac{-n\,k_z}{R}\right)\frac{1}{4\pi jR}\,\frac{e^{-j\Delta\sqrt{k^2-(n/R)^2-k_z^2}}}{\sqrt{k^2-(n/R)^2-k_z^2}}$$

$$\tilde{H}_\phi\Big|_s = \frac{Q}{2\pi\eta jk}\left(-\frac{n^2}{R^2}+k^2\right)\frac{1}{4\pi jR}\,\frac{e^{-j\Delta\sqrt{k^2-(n/R)^2-k_z^2}}}{\sqrt{k^2-(n/R)^2-k_z^2}}$$

where Q is a constant.

The total field on the cylinder can then be expressed as

$$\overline{H}(Q) = \overline{H}_{PLANAR}(Q) + \overline{H}_{DIFFERENCE}(Q) \qquad \text{(Eq. 2.0-9)}$$

where $\overline{H}(Q)$ is the total field as predicted by an asymptotic solution, and $\overline{H}_{PLANAR}(Q)$ is the field that would exist on a flat, infinite ground plane. (It may be thought of as taking the planar field, "wrapping" it around the cylinder, and subtracting it from $\overline{H}(Q)$). The transform of the surface fields is given by

$$\tilde{\overline{H}}(n,k_z) = \tilde{\overline{H}}_{PLANAR}(n,k_z) + \tilde{\overline{H}}_{DIFFERENCE}(n,k_z) \qquad \text{(Eq. 2.0-10)}$$

and $\tilde{\overline{H}}_{PLANAR}(n,k_z)$ is given analytically above. $\overline{H}_{DIFFERENCE}(Q)$ is at most on the order of $1/\sqrt{s}$, so that evaluation of $\tilde{\overline{H}}_{DIFFERENCE}(n,k_z)$ can be reliably obtained from application of the FFT. Any test which involves breaking the fields up into planar and difference fields will be termed a <u>hybrid</u> computation, because it combines analytic and numerical techniques. The only difference between a "hybrid computation" and a "direct computation" is in the method of obtaining the spectrum. After the spectrum is found, both tests proceed

identically. Figures 2 and 3 compare the phase of $\tilde{H}_\phi$ for a fixed value of k_z, when the transform was derived from hybrid and direct computations. Comparison with the phase of the modal transform reveals the increased accuracy of the hybrid method.

Note that the analytic transform presented above arises from a doubly infinite integral, i.e., it is essentially a continuous transform. The periodicity in ϕ is imposed by sampling the continuous transform. The rationale behind such an approach lies in the argument that at $\phi = \pm\pi$ the H-fields are negligible compared to the field at the origin, so the extension to a continuous transform introduces negligible error. The infinite nature of z is preserved and handled exactly.

For the E-field test the three asymptotic solutions are compared to an exact modal solution [2]. The procedure used in deriving the exact modal solution is essentially the same that is used to perform the E-field test. The difference lies in the fact that while the test begins with the asymptotic H-field, the modal solution begins with the known E-field (known for an elemental source). In a manner similar to the test, the H-spectrum may be found from the known E-fields and be expressed in terms of the E-spectrum. This provides analytic H_z and H_ϕ spectrums that can be compared to those resulting from the asymptotic solutions. After the H-spectrum is obtained from the E-field, it may be tested just like any other spectrum. This "check," which begins with a surface E-field, finds the H-spectrum and then returns to the surface E-field, is also valuable in assuring that the FFT sampling of the spectrum is sufficient.

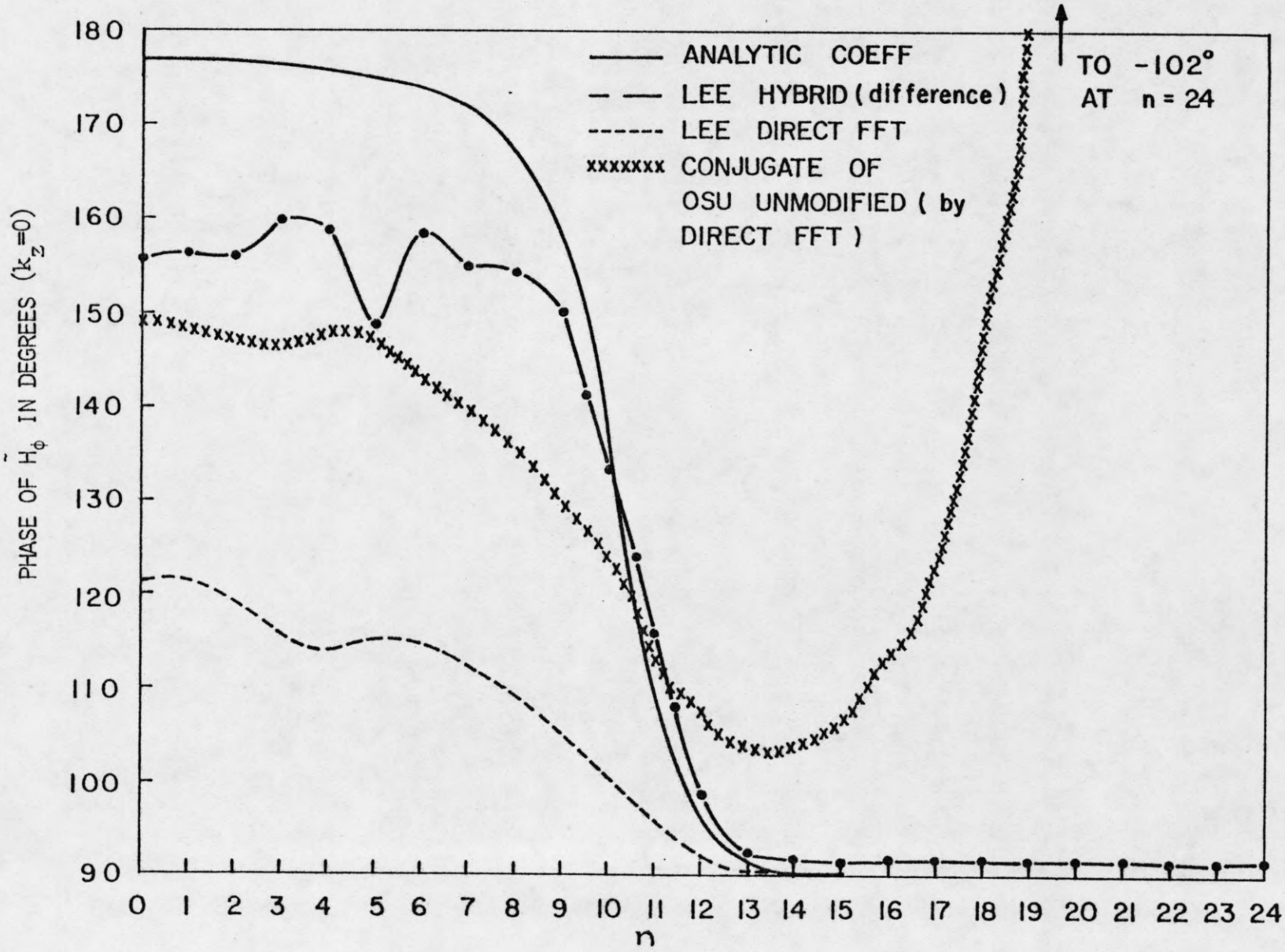

Fig. 2. Phase of $\tilde{H}\phi$ For kz = 0

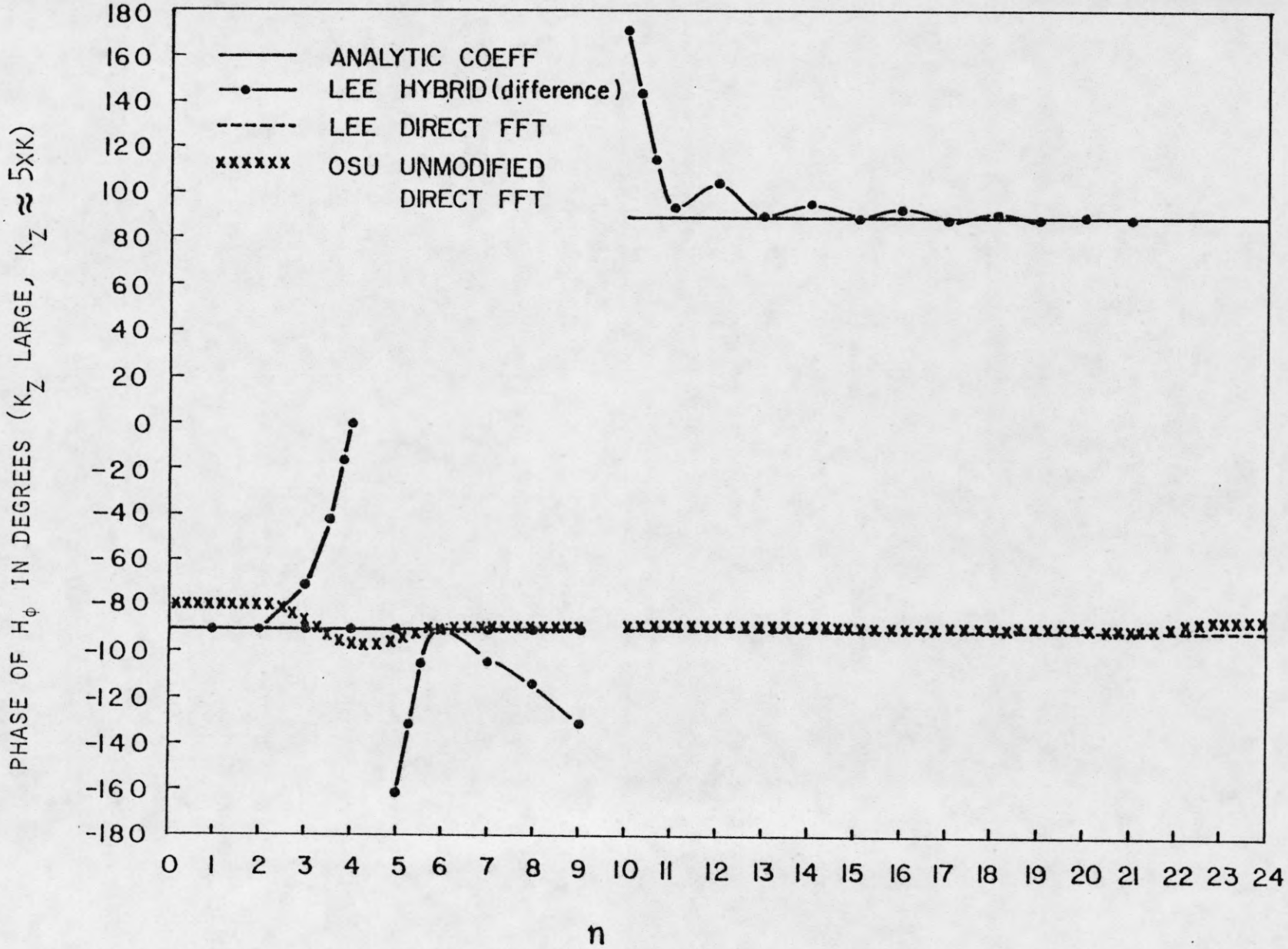

Fig. 3. Phase of $\tilde{H}\phi$ For kz, Large

During actual application of the test, the source used was a slot radiator instead of an elemental dipole. This was necessary because the surface E-field of the slot is finite, although discontinuous, while the surface E-field from the elemental source is singular. Sampling the E-spectrum sufficiently well to represent the singular surface field would make the computer requirements prohibitively large, while the more regular slot is readily handled.

Representation of the slot spectrum was achieved by first determining the H-field spectrum due to an elemental dipole source (the direct asymptotic solutions or, for the analytic case, $\bar{E}_{SURFACE} = \hat{z}\,\delta(\rho-R)\,\delta(\phi)\,\delta(z)$). The H-spectrum was then multiplied by the transform of the slot distribution, which is equivalent to convolving the elemental source with a distribution in the space domain. For a finite slot as shown in Fig. 4a the transforms used were of the form $[\sin(k_z b/2)]/(k_z b/2)$ to represent a rect function (Fig. 4b) in the z-direction, and of the form $\cos(\alpha n)/[\pi^2/4 - (\alpha n)^2]$, $\alpha = \arcsin(a/2R)$ to represent a cosine-like spreading in ϕ.

This then constitutes the totality of the E-field check. The components of the spectrum of the H-field that result from an elemental source are determined. For the asymptotic solutions the spectrum is determined either by direct application of the FFT or by use of the hybrid technique; for the exact case the H-spectrum may be found analytically. Regardless of its source, the H-spectrum is then multiplied by the transform of the assumed slot distribution, accomplishing the convolution that is necessary to represent the slot

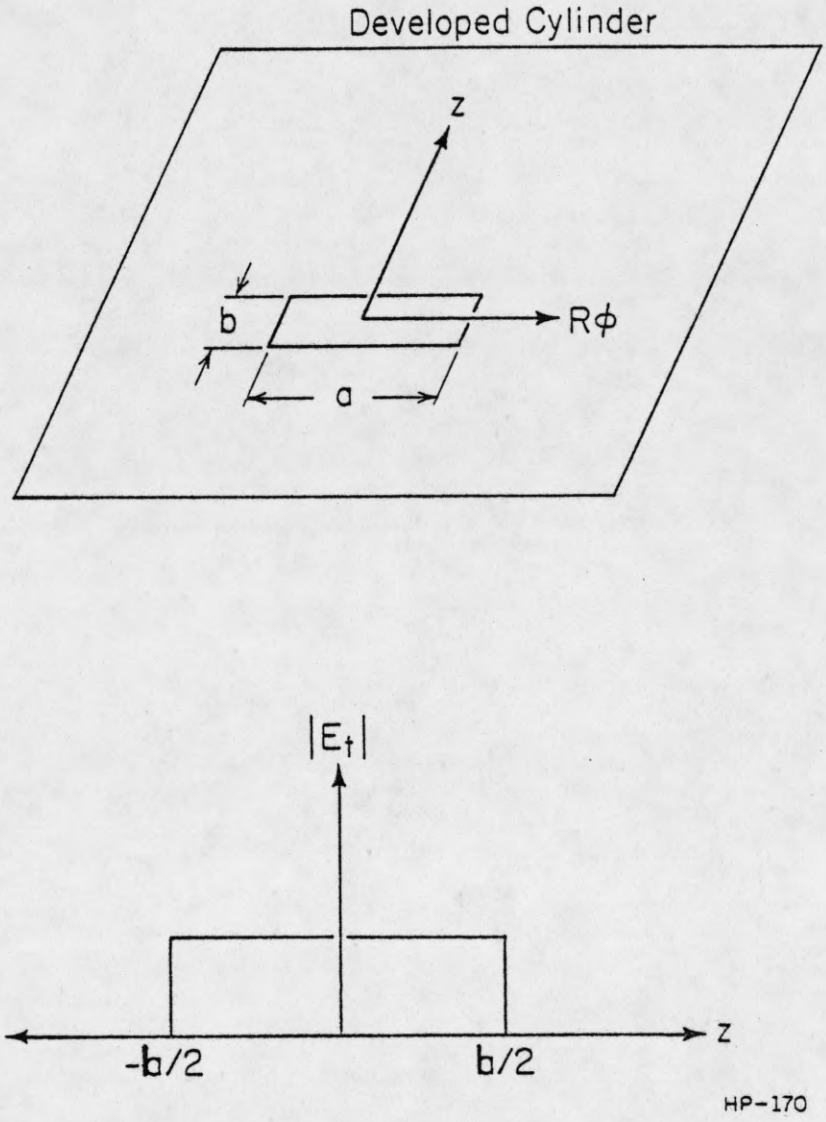

Fig. 4. Slot Geometry.

distribution. The E-field spectrum is then found from modification and combination of the H-field spectrum components. Finally, inverse Fourier transformation and summation of the Fourier coefficients give the surface E-field. The next section compares the surface H-fields given by the three asymptotic solutions and compares their H-spectrums and surface E-fields to that resulting from the analytic solution.

2.1 Results of the E-Field Test

All results presented here are for the following configuration:

Cylinder radius R = 1.517 λ

Slot width b = .3048 λ

Slot length a = .6858 λ

Extent of z sampling = 12.5 λ

Number of samples in z = 128

Extent of ϕ sampling = 2π radians

Number of Fourier coefficients in ϕ = 64.

This set of parameters results in a sampling of the spectrum out to $k_z \approx 5*k$.

The figures that follow are three-dimensional views of the surface H-field due to an elemental source, the H-spectrum resulting from an elemental source, and the surface E-field that results from carrying out the test. The surface E-field is calculated after multiplication by the spectrum of the assumed slot distribution, so E_ϕ should be zero everywhere and E_z should have value only in the extent of the slot. These plots are more valuable in representing shape and form than in revealing magnitude values. One should be especially wary of reading

peak magnitudes, because the plot program sets all values outside a specified range to the peak value. Thus, when a plot should actually extend outside the plot boundaries, the action of the plot program is to make it appear as a "flat-topped" curve at the peak value. Since all of the magnitudes are symmetric in z and k_z, only half of the total surface is presented in each plot.

Fig. 5 shows the surface E-field that results from application of the test to the analytic H-spectrum. This is the standard to which all the other solutions will be compared. The analytic solution results in an E_ϕ that is essentially zero (the totally flat curve) and an E_z that is well contained. The fact that E_z goes to zero in a smooth curve in the z-direction instead of a discontinuous curve is due to the numerical calculation. It is this curve that reveals that the error introduced by performing finite sums and integrals is negligible.

Figure 6 presents results from a direct application of the FFT to the UI solution. Figures (a) and (b) present the total surface H-field. It should be noted that these figures have been artificially flat-topped by the plotting program, and the actual peaks are two orders of magnitude greater than the values plotted. This graphically shows how very peaked the fields are that the FFT was attempting to transform. Figures (c) and (d) show the surface E-fields. The E_z field is considerably more spread than the analytic case. The E_ϕ field, instead of being zero, shows two sharp peaks near the source and a rippled character away from the source. Figure 7 presents the same curves, except that the viewing angle in the plane of the surface

has been shifted by 180 degrees, i.e., the surface has been rotated by 180 degrees and one now views the "other side."

The effect of using a hybrid computation on the UI solution can be seen in Figure 8. Here (a) and (b) show only the difference current, i.e., the current left over after the planar current has been removed. This dramatically shows how much less "peaky" the difference current is, for here there is no artificial flat-topping (the scale is the same as for the direct test). What remains in H_ϕ is the $1/\sqrt{s}$ term at the origin, while the H_z is greatly reduced everywhere. The beneficial effects of using the hybrid computation are easily seen in the E-fields of (c) and (d). Here the form of E_z (c) is much closer to the analytic shape than when the direct FFT was used, and the peaks of E_ϕ (d) have been removed entirely. E_ϕ still retains some of its rippled character, but overall it has been greatly reduced. Figure 9 presents the same curves with the viewing angle changed by 180 degrees.

Since the previous four figures reveal the desirability of using the hybrid computation when possible, the results of testing the OSUMOD solution by direct FFT are not shown. Applying the hybrid method to the OSUMOD solution generates the forms of Figure 10. Figures (a) and (b) show only the difference current. Here H_ϕ goes to zero at the origin since the OSUMOD and planar solutions are identically the same and no $1/\sqrt{s}$ term is present; the H_z difference field is very similar to that of the UI solution. The E-fields resulting from the hybrid computation applied to the OSUMOD solution ((c) and (d)) are practically indistinguishable from those of the UI

solution. This point will be covered more thoroughly in the next section. Again, Figure 11 shows the same curves with a 180 degree different view.

Because the OSU solution only has a singularity (peak) on the order of 1/s, it is not necessary to resort to a hybrid computation to obtain a reliable check. Figures 12 (a) and (b) show the total surface H-field (not the difference field). As in the direct UI test, these curves have been flat-topped by the plotting program so that the true peak is much higher than appears here. Figures (c) and (d) present the resulting surface E-field. As can be seen, the extent of the E_z field is much broader than that of the modal solution, and the E_ϕ field has significant non-zero content. The viewing angle has been changed by 180 degrees for Figure 13.

While the three-dimensional plots are good for determining the overall trend and elucidating the general shape of curves, it is often difficult to use them to get specific information about a single point or constant coordinate cut. The point of interest may, for example, be hidden behind a peak which obscures it from view. Accordingly, Figure 14 is a graph of the resultant E_z field along the $\phi=0$ cut, i.e., through the slot and along the cylinder axis. There are several features of interest here:

1) The analytic solution predicts well the expected discontinuity in E_z.

2) The UI and OSUMOD solutions checked with the hybrid computation are indistinguishable from one another. Their E_z field is slightly more spread than that of the analytic solution.

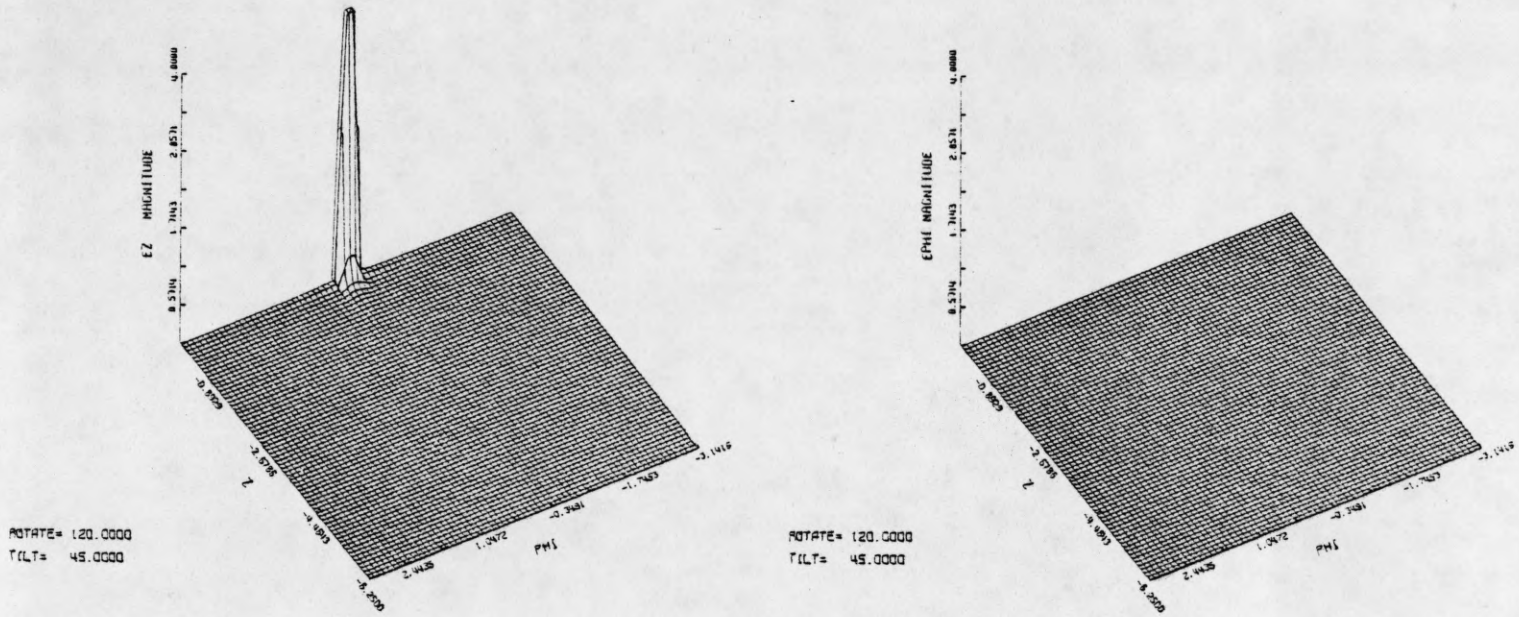

(a) (b)

Fig. 5. E-Field Test: Analytic $\tilde{H}$.

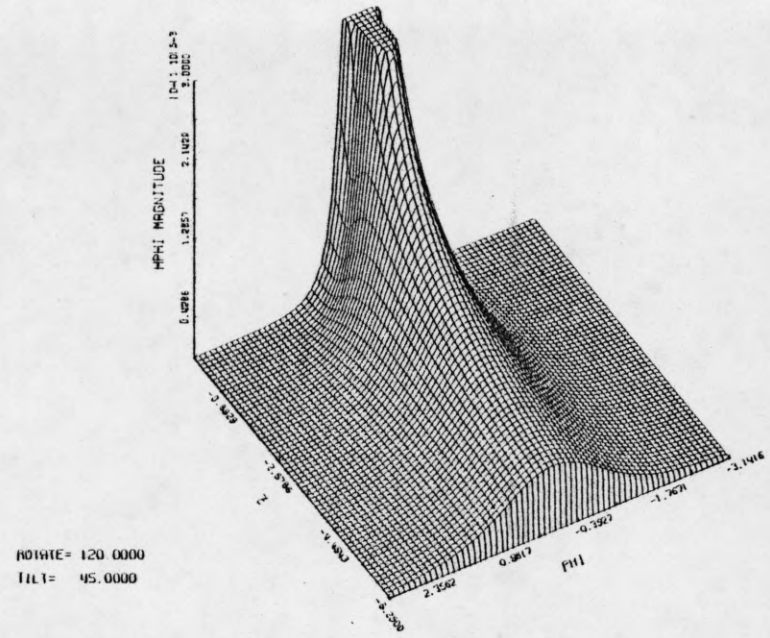

(a)

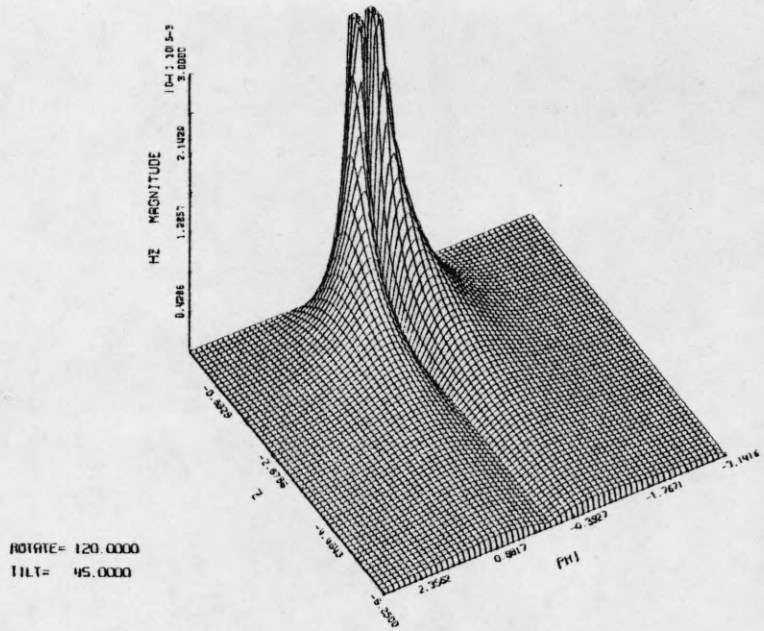

(b)

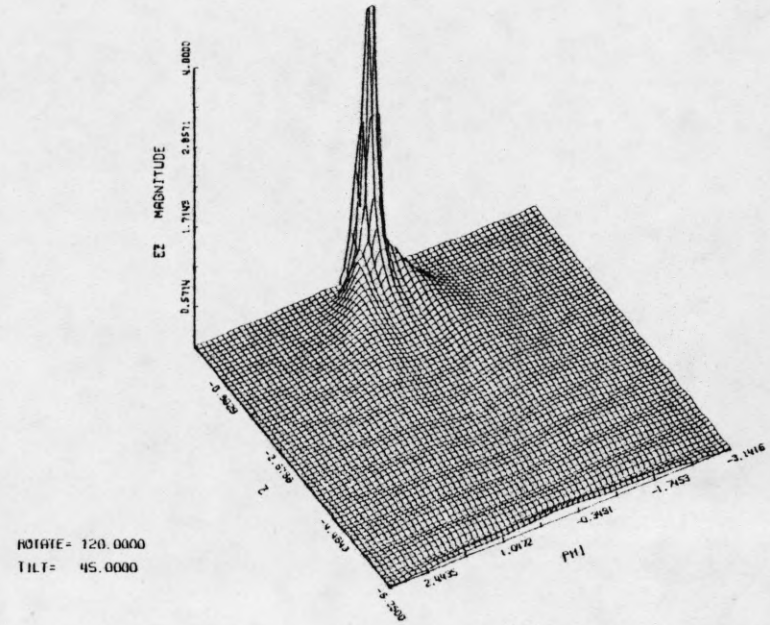

(c)

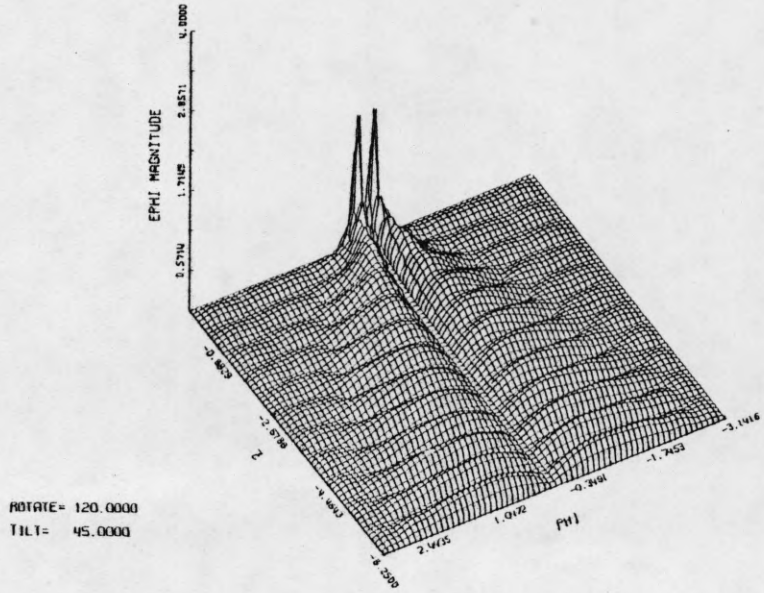

(d)

Fig. 6. E-Field Test: Direct Test of UI Solution.

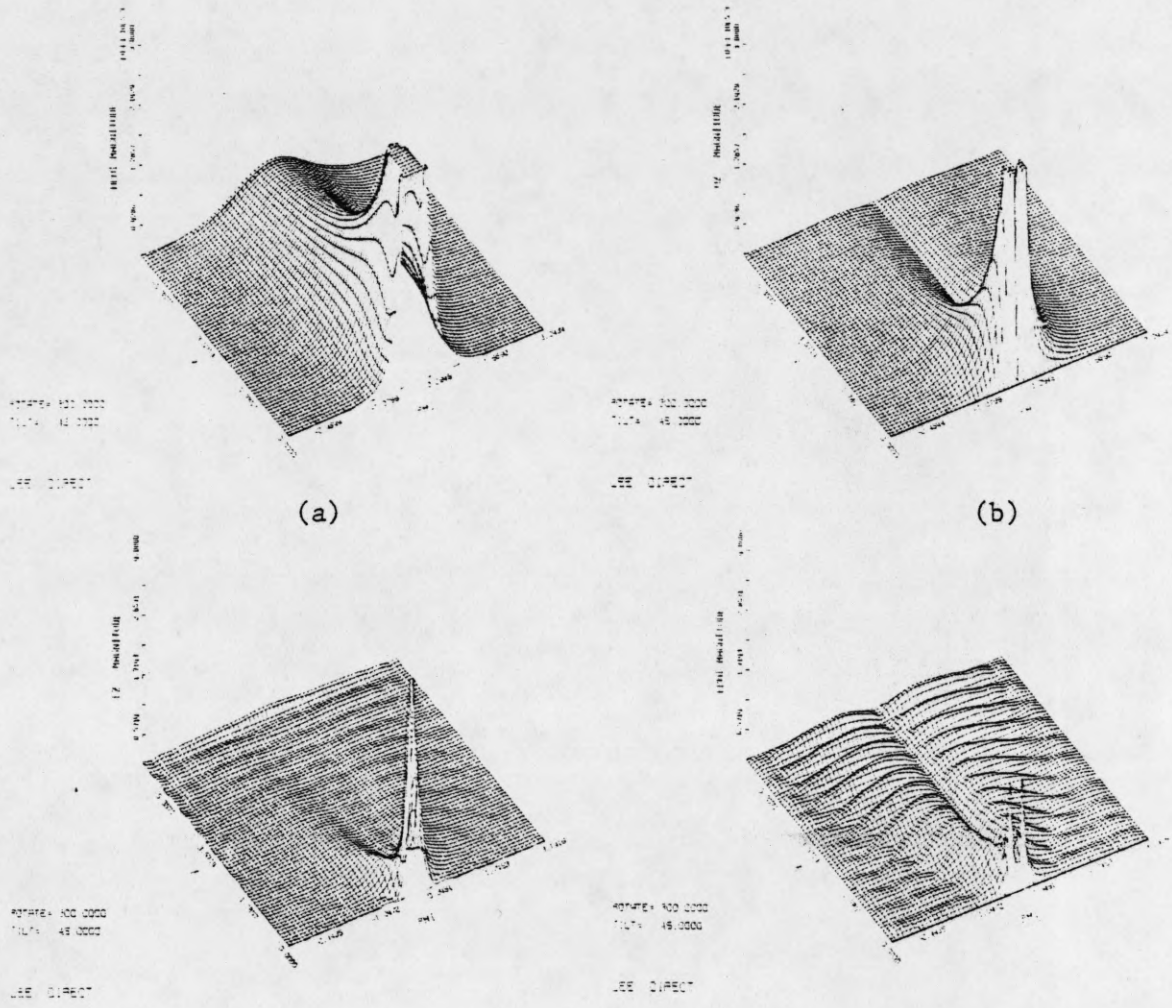

(a) (b)

(c) (d)

Fig. 7. E-Field Test: Direct Test of UI Solution.

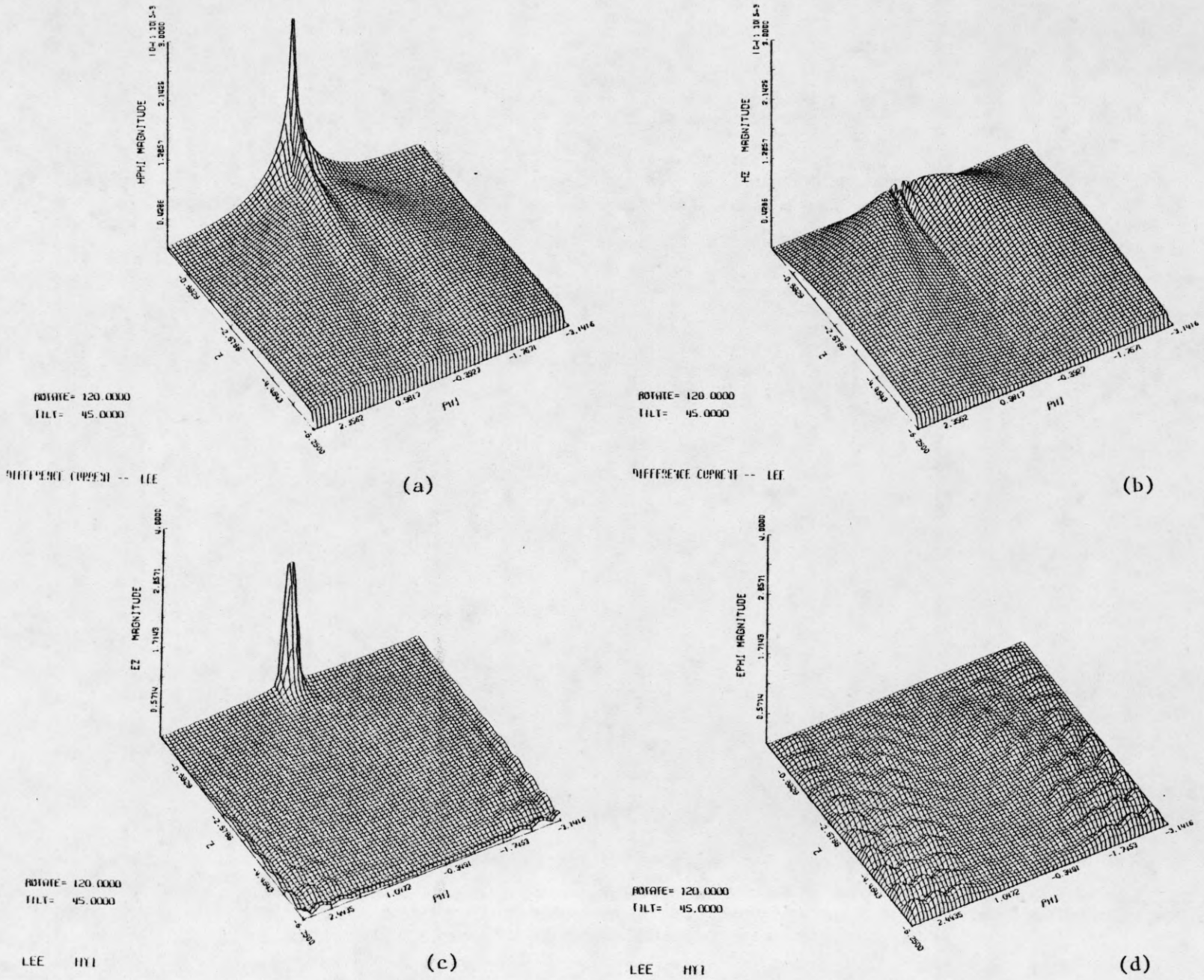

Fig. 8. E-Field Test: Hybrid Test of UI Solution.

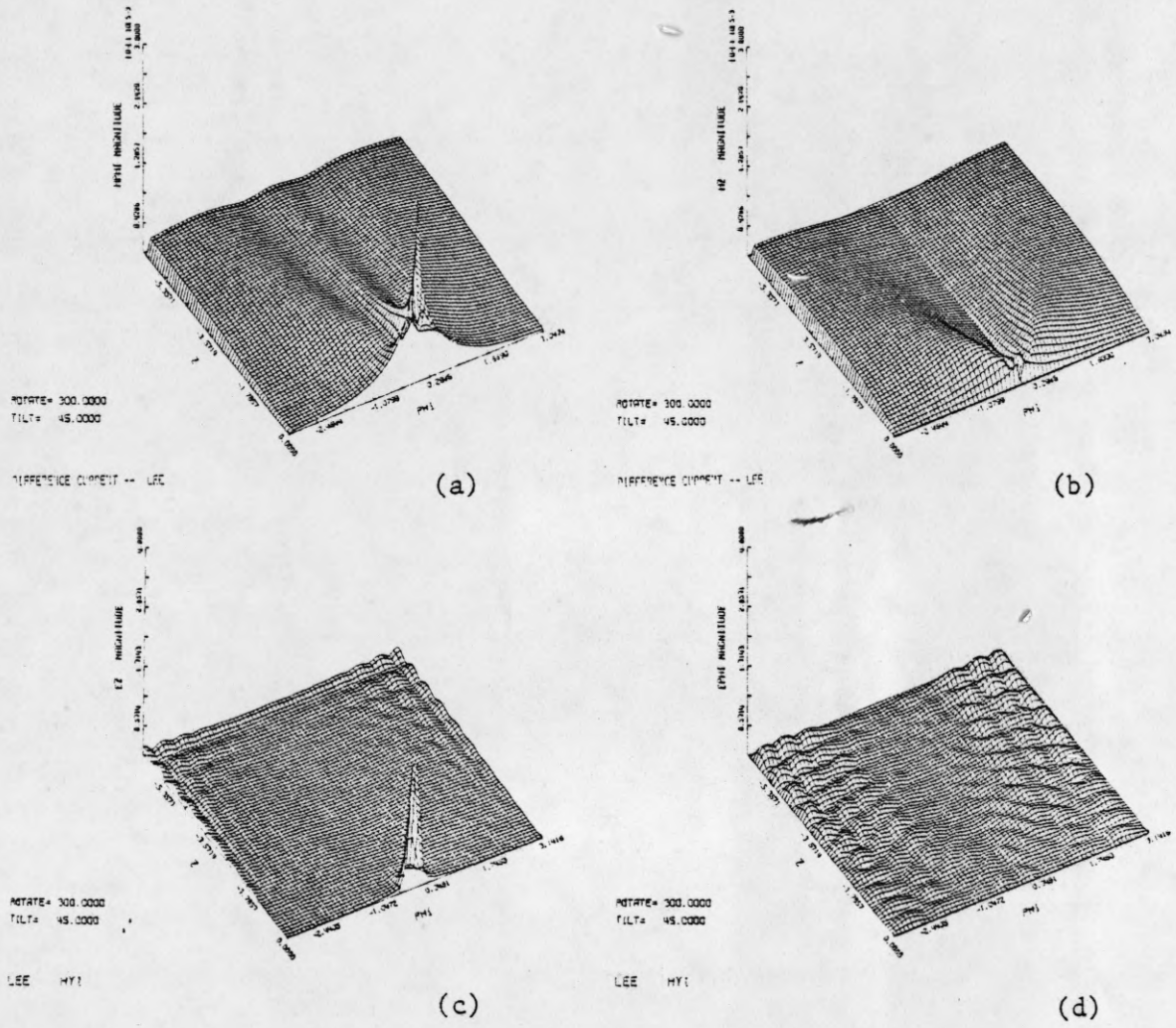

Fig. 9. E-Field Test: Hybrid Test of UI Solution.

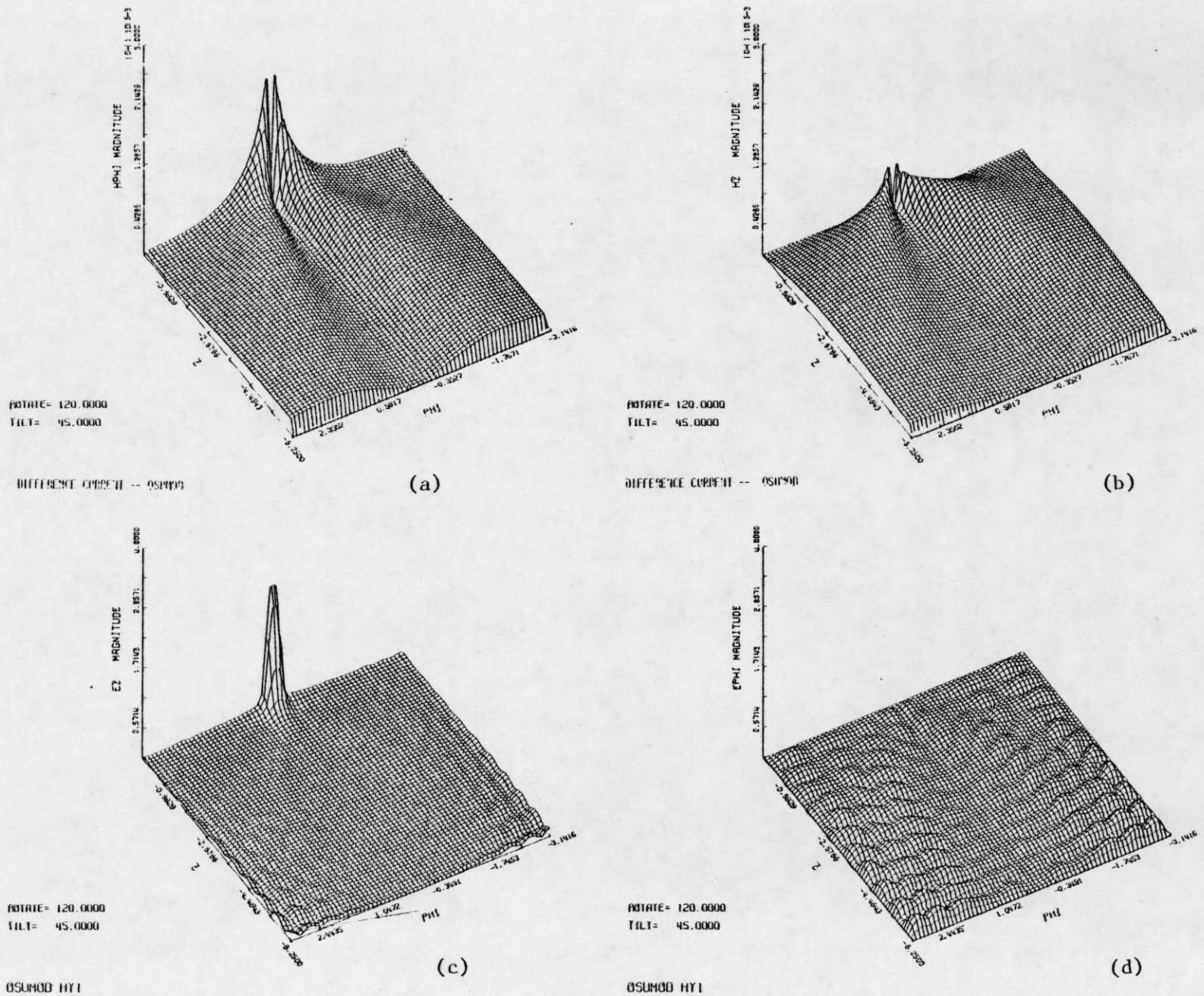

Fig. 10. E-Field Test: Hybrid Test of OSU Mod Solution.

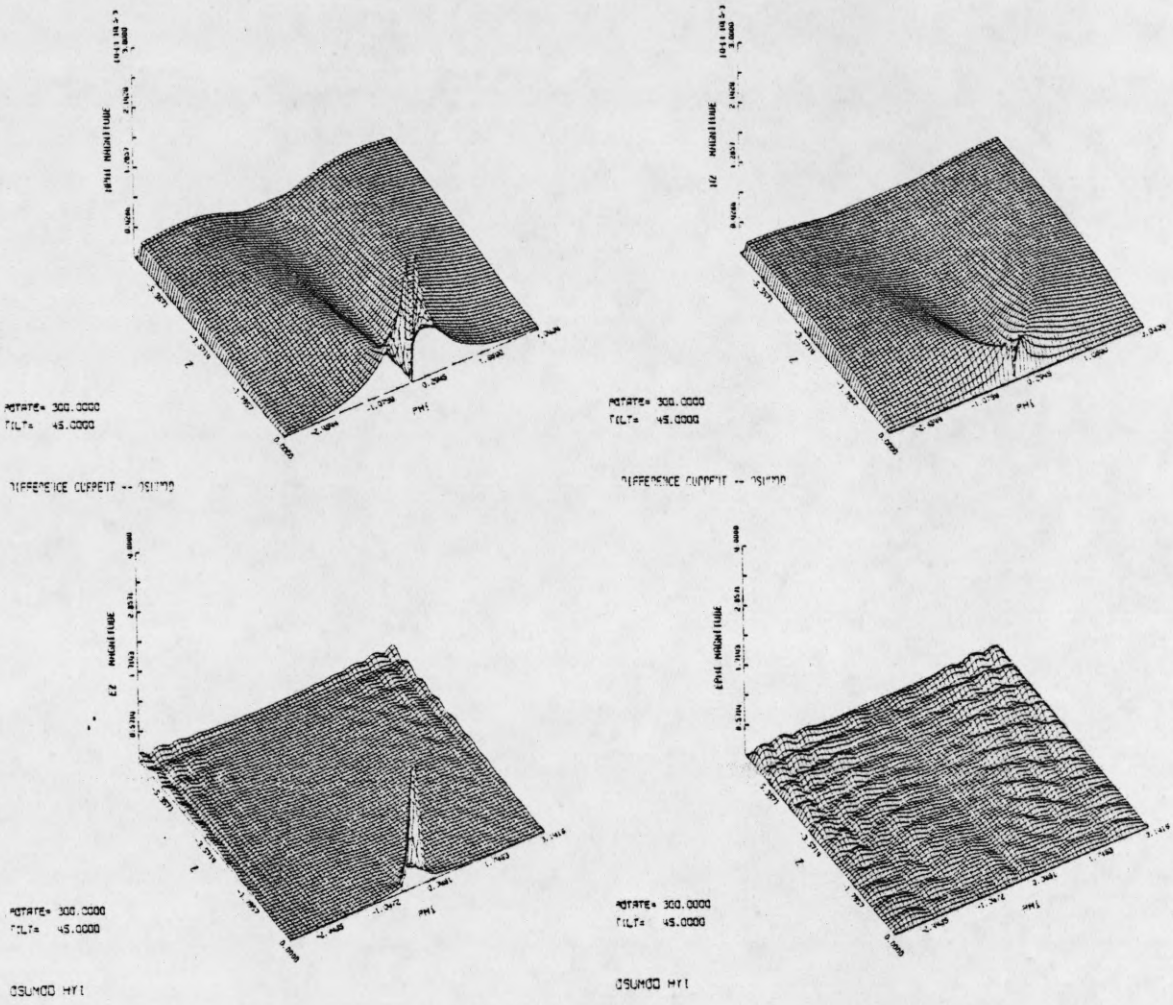

Fig. 11. E-Field Test: Hybrid Test of OSU Mod Solution.

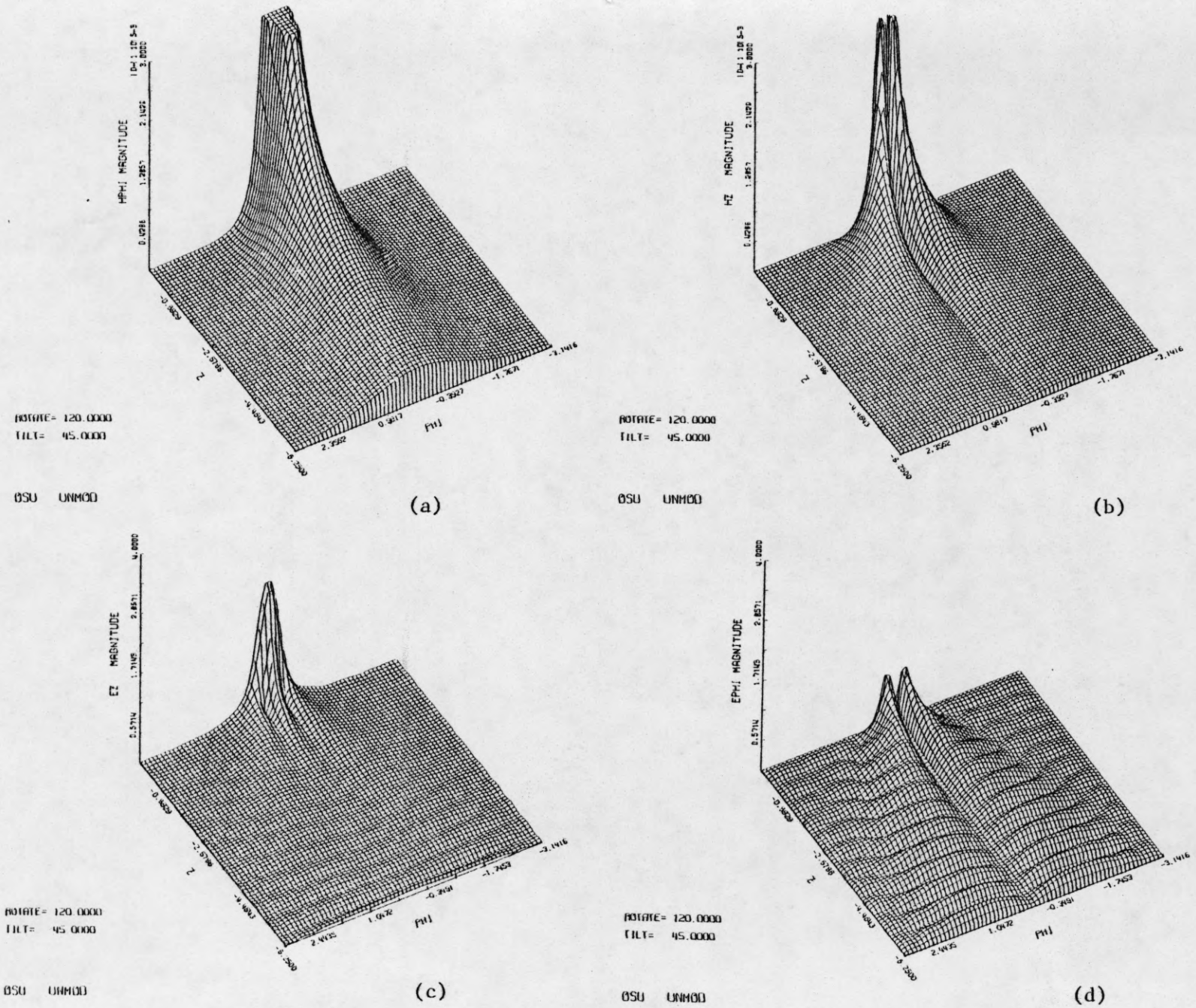

Fig. 12. E-Field Test: Direct Test of OSU Solution.

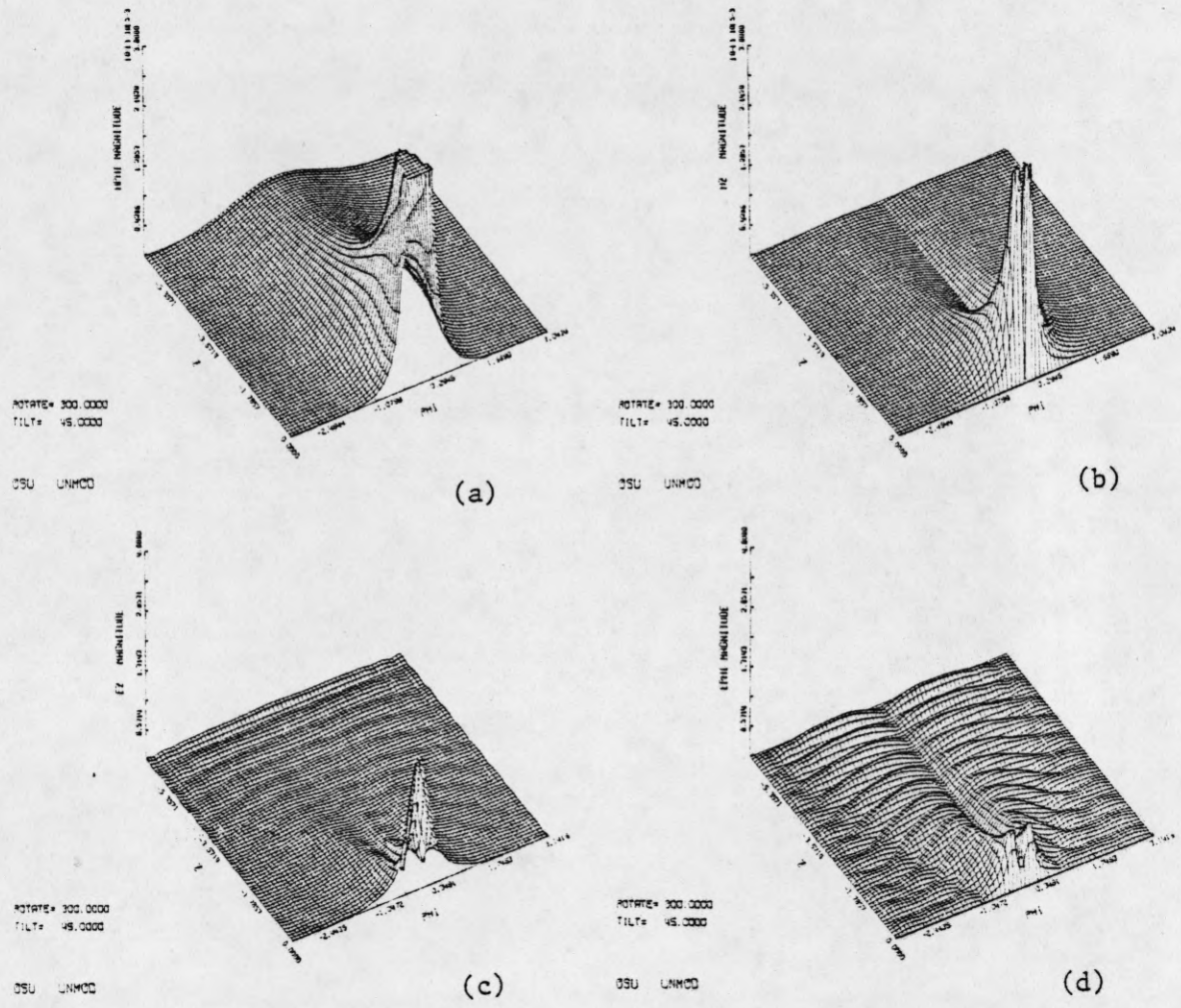

Fig. 13. E-Field Test: Direct Test of OSU Solution.

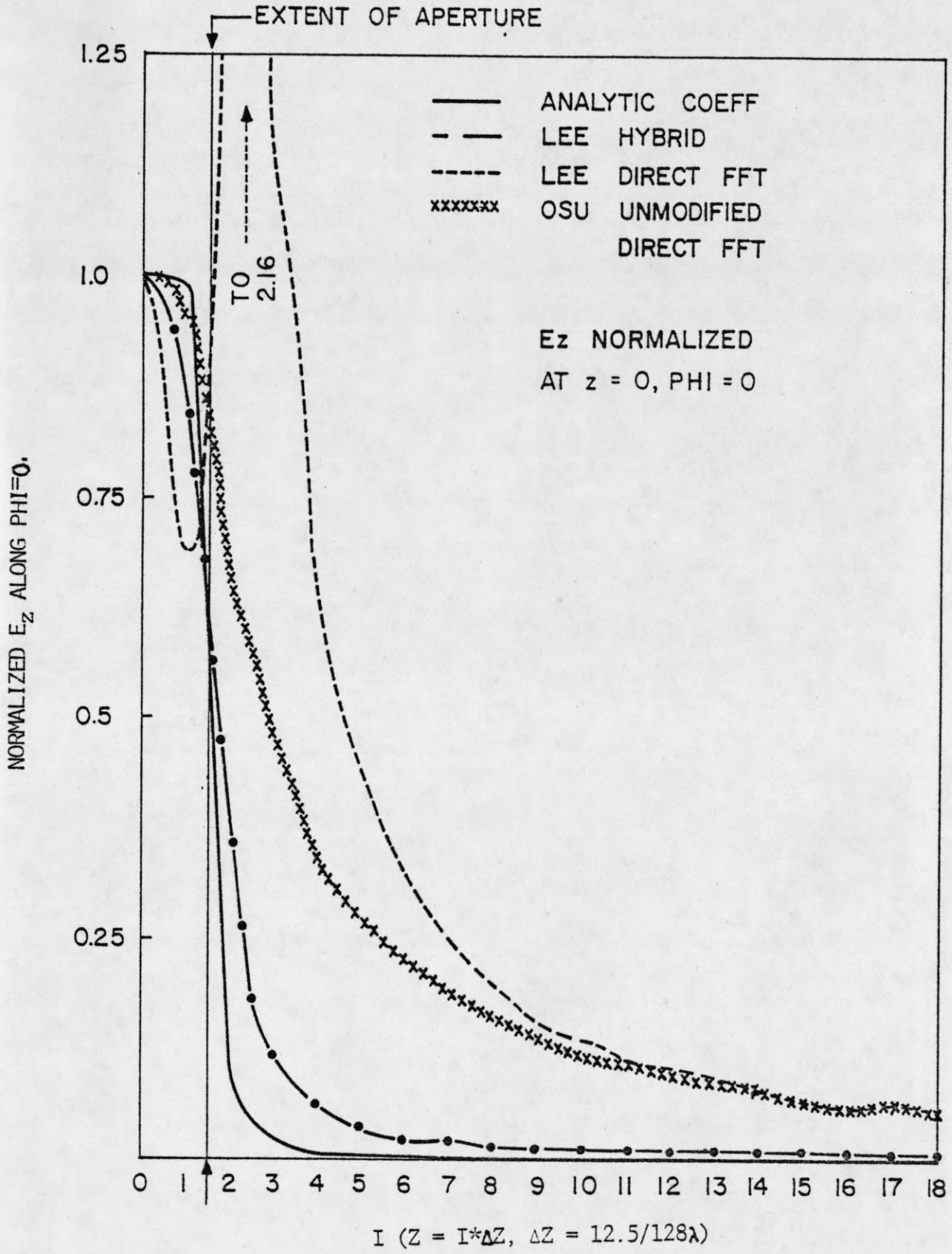

Fig. 14. Surface E_z Along $\phi = 0$

3) The OSU solution with a direct test does attain the desired shape curve, however, it has significant E_z content over a much larger region than either the UI or OSUMOD solutions (where E_z should be zero).

4) The direct computation applied to the UI solution yields a sharp peak at the edge of the slot. The large field values extend outside the slot region where the field should go to zero.

The three-dimensional plots concealed the local behaviour at the edge of the slot resulting from a direct computation of the UI solution. This ϕ=0 cut, however, shows dramatically the improvement when a hybrid computation is used.

Figures 15 through 19 compare the spectrum of the surface H-field resulting from an elemental dipole. In each plot both the H_ϕ and H_z spectrums are shown as viewed from two different angles. The primary differences to be seen are that for the H_ϕ spectrum none of the asymptotic solutions yields the relatively large values for large n and k_z that the analytic solution does. Also, the analytic spectrum is, in general, smoother than the others. It is also apparent that the direct FFT applied to the UI solution has the effect of "digging a trench" around the peak. Comparison with the analytic solution shows this to be clearly in error.

The H_z spectrum yields somewhat less interesting curves. Again the analytic solution has relatively larger values than any of the asymptotic solutions. Curiously, the analytic, OSU, and the UI solutions with direct FFT are relatively smooth, while the peaks of the hybrid computations are less regular.

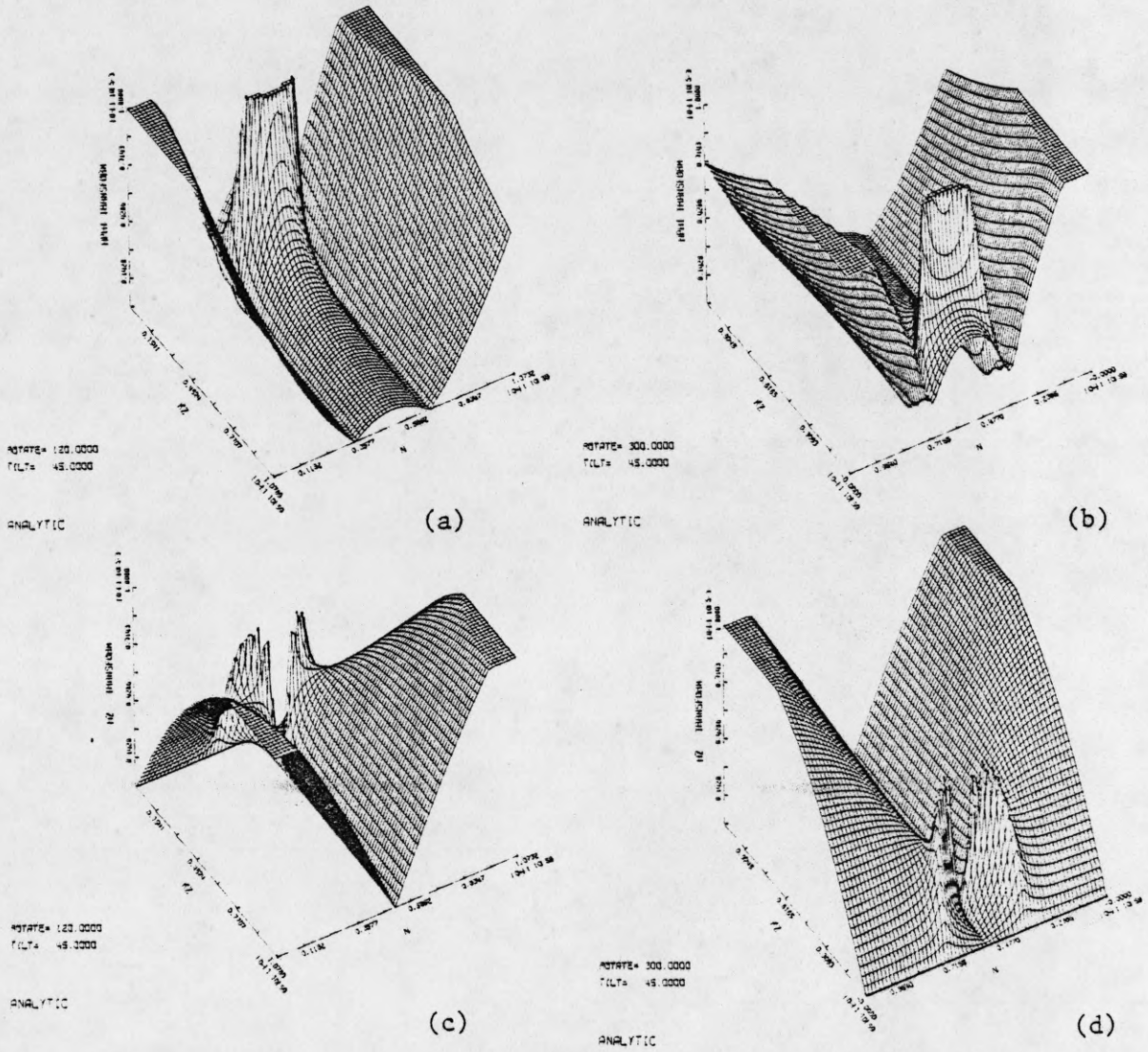

Fig. 15. Spectrum of H: Analytic.

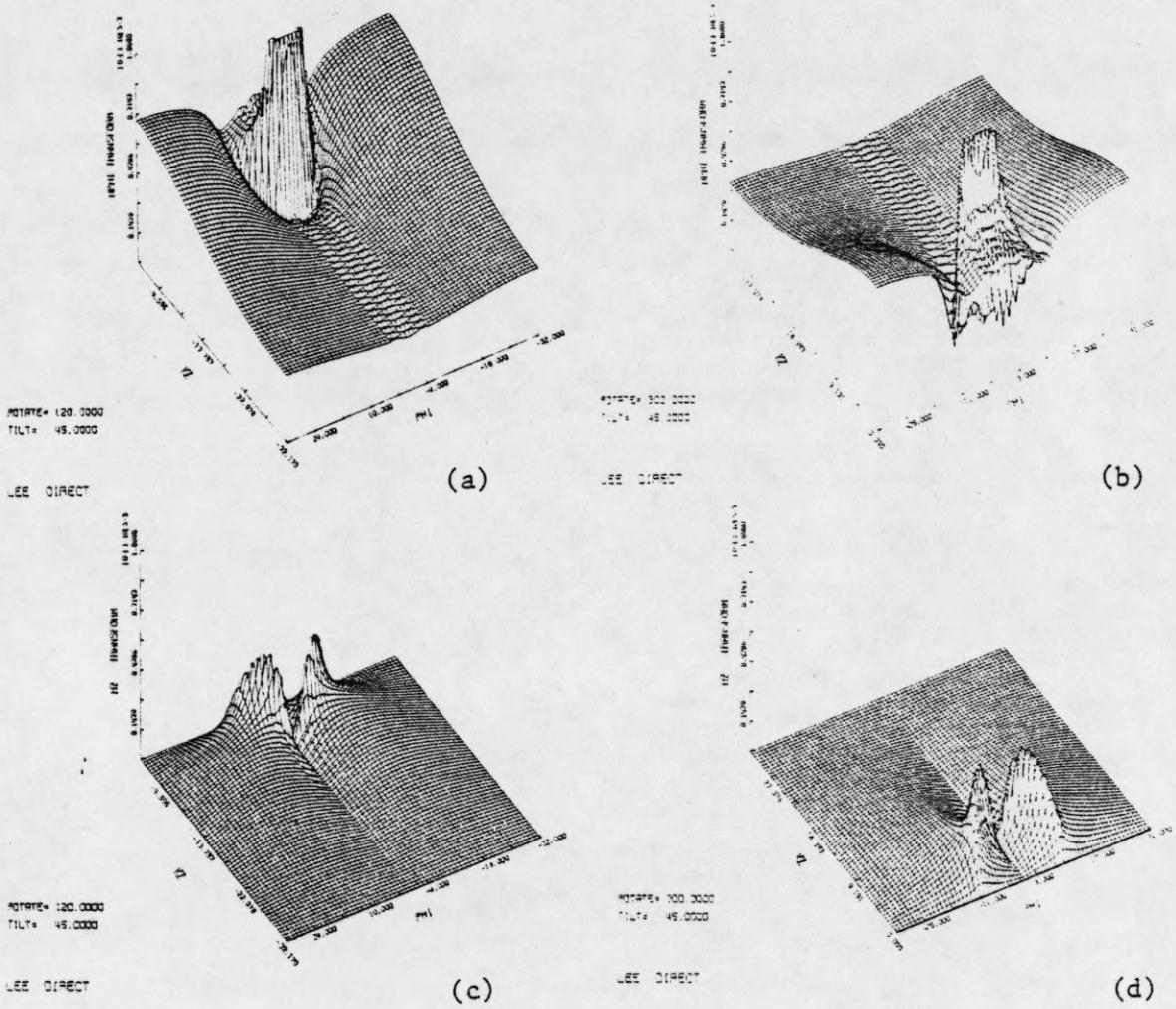

Fig. 16. Spectrum of H: Direct Test of UI Solution.

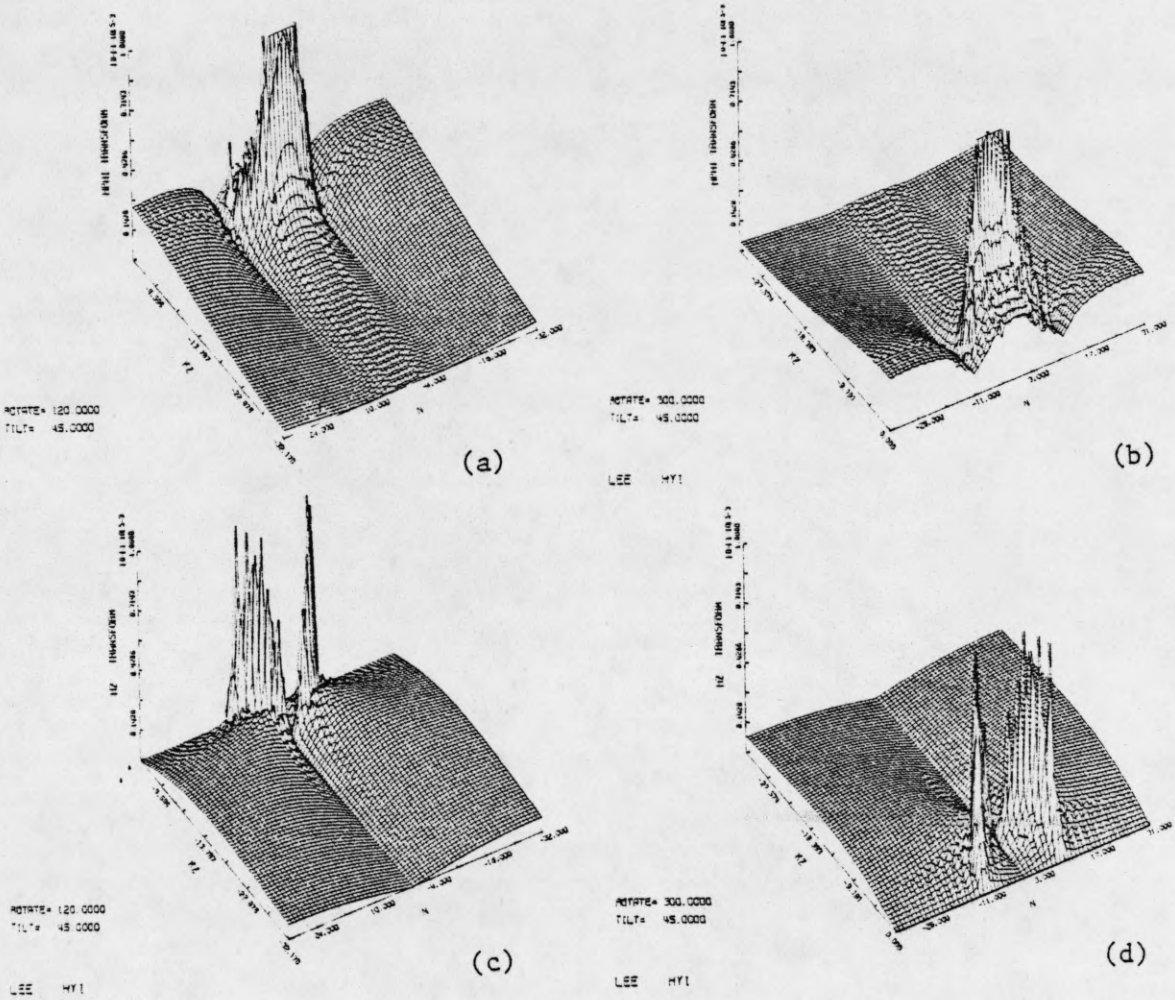

Fig. 17. Spectrum of H: Hybrid Test of UI Solution.

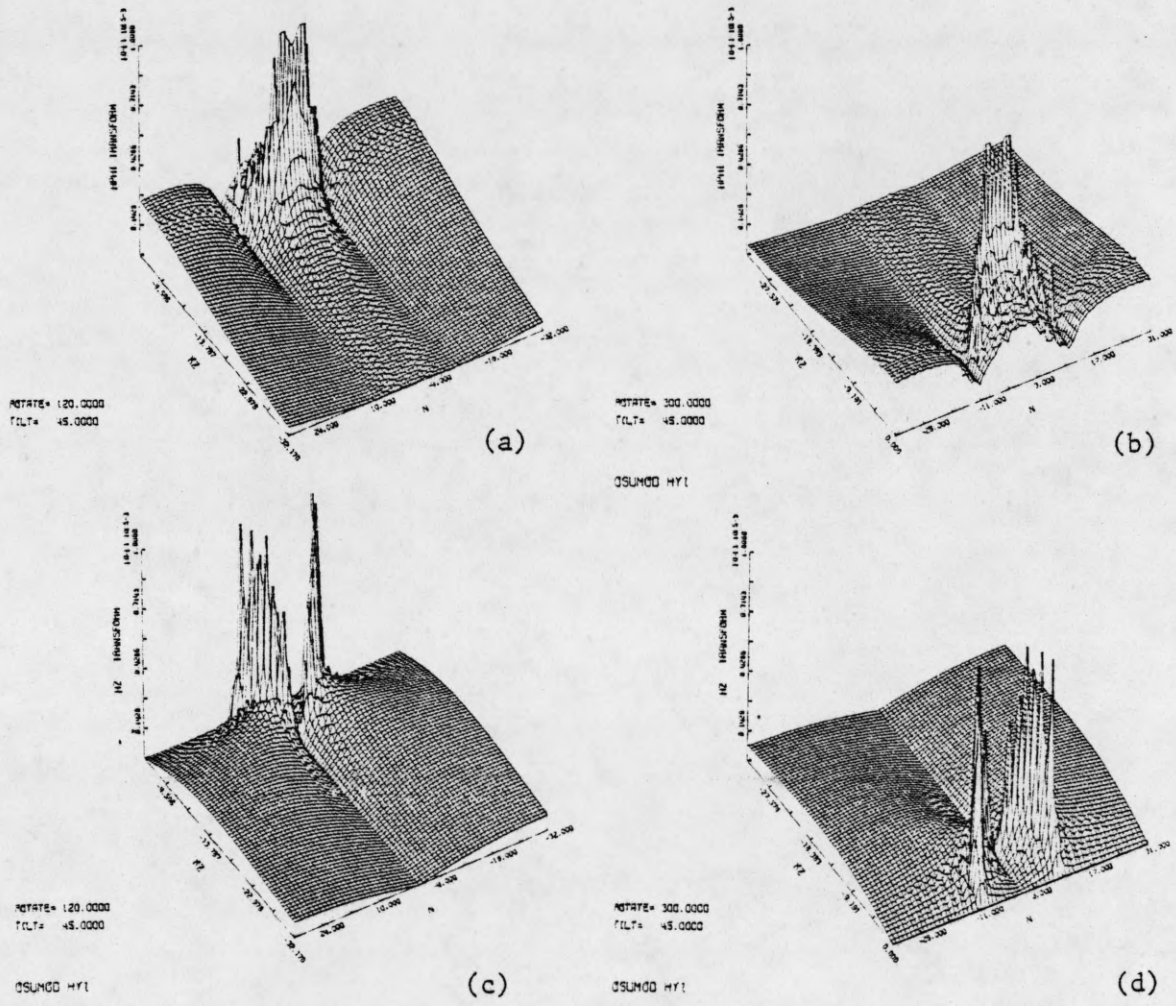

Fig. 18. Spectrum of H: Hybrid Test of OSU Mod Solution.

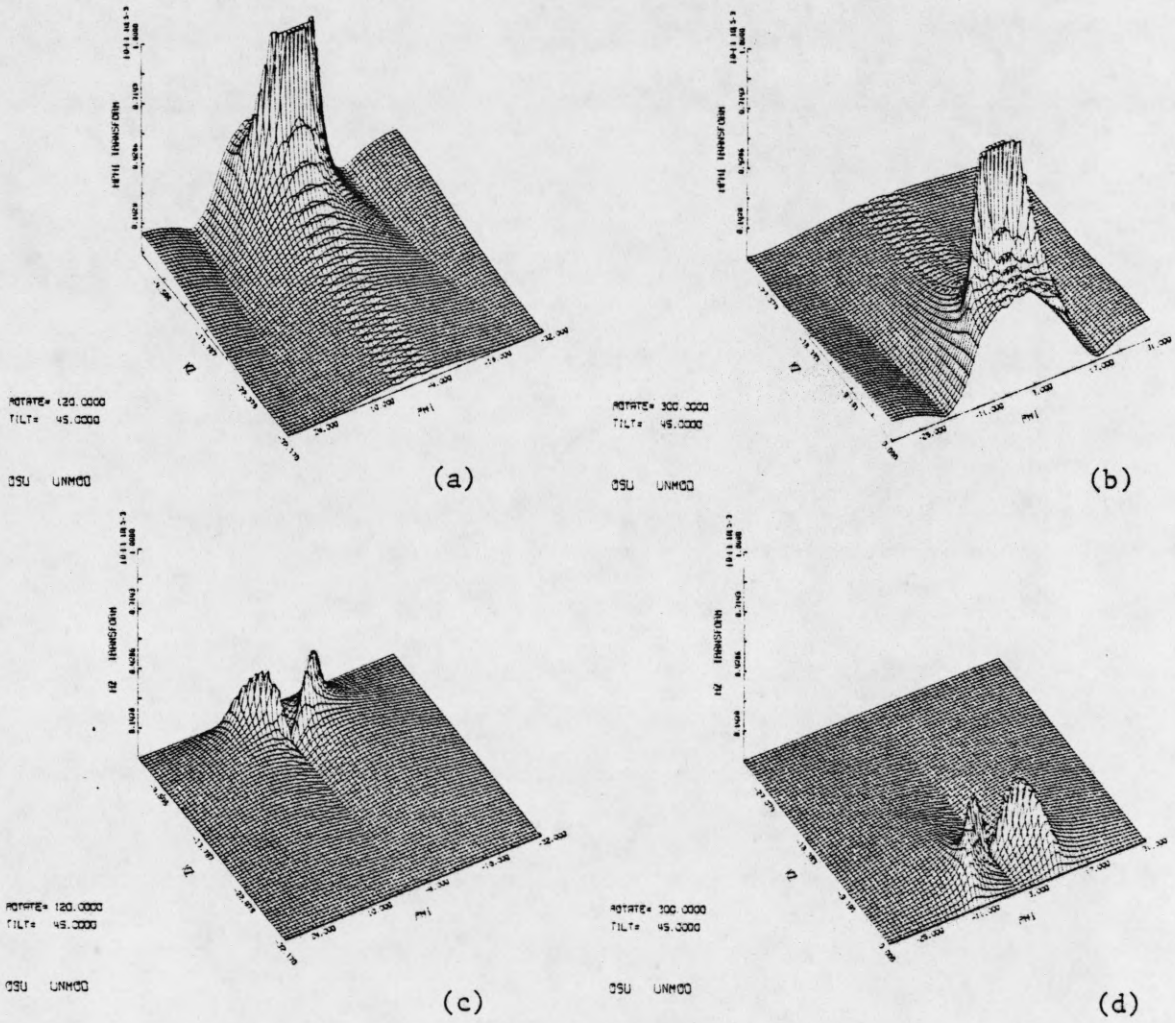

Fig. 19. Spectrum of H: Direct Test of OSU Mod Solution.

In review, this section has presented three-dimensional views of the surface H-field, H-spectrum, and the resulting surface E-field for all the asymptotic solutions tested. Two different viewing angles are provided and, where applicable, the plots of the analytic modal solution were included. Auxiliary graphs were used to clarify specific points.

2.2 Discussion of E-field Test

In beginning the E-field test, it was hoped that this would provide a means of reliably judging the accuracy of asymptotic solutions. It was also hoped that application of the test would reveal the role of the source region behaviour in satisfying the test, and that the test would differentiate between solutions characterized by on-axis behaviour that decayed as $1/s$ and $1/\sqrt{s}$.

The effect of the E-field test in fulfilling these wishes has been mixed. The resulting E-field does provide a good qualitative measure of how well the asymptotic solution satisfies the E-field boundary condition. A quantitative measure could be devised from the test by calculating the percentage of energy in the E-field that lies outside the slot aperture. In this case, a perfect solution would, of course, test to zero percent.

The E-field test does provide information about the source region -- asymptotic solutions that contain higher order terms ($1/s^2, 1/s^3$) in the source region H-field do satisfy the E-field test better than solutions that contain only terms on the order of $1/s$. However, the large path length behaviour did not appreciably affect the test

results. If the source region behaviour was the same (for a limiting case), then a solution that decayed as 1/s tested essentially the same as a solution that decayed as $1/\sqrt{s}$. In fact, the surface E-fields that resulted were indistinguishable when graphed, though there were slight numerical differences. In general, it seemed that the energy contained in the long path length region was so small compared to the source region energy that its effect on the results was negligible. The E-field test seems to be most sensitive to the field behaviour where high field values occur. This is not surprising in view of the nature of the E-field test, i.e., based on an integral of the surface H-fields.

Some numerical difficulties were encountered during execution of the test. The high order source-region terms made it quite difficult for the FFT to accurately compute the integral involved. Since use of the FFT requires equally spaced sampling over the interval, a sampling sufficient to accurately evaluate the peak resulted in matrix sizes too large for some computers (CDC CYBER 74, for example). For solutions whose source-region behaviour went to a planar-type singularity in the limit, however, analytic evaluation of the planar spectrum allowed completion of the test. A solution which contains higher-order source region terms but does not go to planar-type behaviour in the limit will be quite difficult to test by this method unless it has an analytical transform (or unless the investigator has an extraordinarily large computer).

The PINY solution is a good example of this, for it contains the $1/s^2$ source region term, but not the $1/s^3$ term. The PINY solution could be

tested by modifying its source region behaviour by the addition of the $1/s^3$ term and performing a hybrid computation. This has not been done since comparison of the OSUMOD and UI tests indicates that solutions with the same limiting source region behaviour will yield virtually identical E-field tests.

To sum up, it appears that the E-field test can provide a measure of the accuracy of a proposed asymptotic solution. An FFT is employed so that the evaluation of the integrals involved may be efficiently performed, but some care must still be taken in the computation. The test reveals that solutions which have planar-type source region behaviour in the limit satisfy the E-field boundary condition better than those that only have terms on the order of 1/s. The test is, however, relatively insensitive to the large path length behaviour of a solution. Wire antennas provide a good analogy, for the source-region behaviour dominates calculation of the the self- and mutual-impedance, and the current behaviour at the end plays less of a role. An E-field boundary condition check of a wire antenna would be little influenced by the current far away from the source, but be source region sensitive. It is not surprising, then, that the E-field check reveals little about the local character of solution, but instead provides more of a global test.

3.0 Lorentz Reciprocity Test

The test reported in the preceding sections involved checking how well the asymptotic solutions satisfied the E-field boundary condition on the cylinder surface. Another approach involves introducing a

known test source and checking to see how well Lorentz reciprocity is satisfied -- this check we will call the Lorentz reciprocity test. While checking for satisfaction of boundary conditions is a well-known way of evaluating the accuracy of solutions, to our knowledge this is the first time that reciprocity has been so employed.

A general statement of Lorentz reciprocity is given by (Eq.3.0-1)

$$-\oint_S (\bar{E}^a \times \bar{H}^b - \bar{E}^b \times \bar{H}^a) \cdot d\bar{s} = \iiint_V (\bar{E}^a \cdot \bar{J}^b - \bar{H}^a \cdot \bar{K}^b - \bar{E}^b \cdot \bar{J}^a + \bar{H}^b \cdot \bar{K}^a)\, dv$$

where $\bar{J}^a, \bar{K}^a$ are the "a" sources and $\bar{E}^a, \bar{H}^a$ their associated fields and likewise for the "b" sources, $\bar{J}^b, \bar{K}^b$. The right-hand integration is carried out over some volume, V, and the left-hand integration over the surface, S, which surrounds and defines V. We will associate the "a" sources and fields with the asymptotic solution being tested and denote them ASY, and associate the "b" sources with the test source to be introduced, denoted TST. All of the asymptotic solutions are predicated on a magnetic dipole source with no electric source, and we will use as a test source only a magnetic dipole and its planar image, so the reciprocity equation may be rewritten as (Eq. 3.0-2)

$$V \quad -\oint_S (\bar{E}^{ASY} \times \bar{H}^{TST} - \bar{E}^{TST} \times \bar{H}^{ASY}) \cdot d\bar{s} = \iiint_V (\bar{H}^{TST} \cdot \bar{K}^{ASY} - \bar{H}^{ASY} \cdot \bar{K}^{TST})\, dv.$$

The "reciprocity volume" defining the limits of integration will be taken as concentric infinite cylinders, one of which lies just outside the surface of the conducting cylinder and the other with infinte radius. Since both the test source (magnetic dipole and its planar image) and the asymptotic solution obey the radiation condition, the contribution from the cylinder surface at infinity is zero. The

asymptotic source will be raised slightly above the cylinder surface so that it falls within the reciprocity volume. The test source will be placed so that it also falls inside the reciprocity volume, but its image falls inside the mathematical surface defining the conducting cylinder, i.e., the test source and its planar image yield a plane of zero tangential E-field which lies tangent to the mathematical surface that defines the conducting cylinder.

The term "mathematical surface that defines the cylinder" is used, because in the formulation of the reciprocity integral, the "a" and "b" sources exist independently and not in the presence of each other. Thus $\overline{E}^a$ and $\overline{H}^a$ are determined totally by the asymptotic solution of a magnetic dipole on an infinite conducting cylinder. Similarly, $\overline{E}^b$ and $\overline{H}^b$ are totally determined by a test magnetic dipole and its planar image radiating in free space with no conducting cylinder and no other sources present. The "a" and "b" fields and sources are brought together only in computation of the integral, where the two independent solutions are combined. It is during this superposition that the test sources are placed so that their plane of symmetry is tangent to the cylinder of the asymptotic problem. This is an application of Generalized Reciprocity where the two sources, "a" and "b," can be totally independent as long as the boundary conditions within the "reciprocity volume" are identical. In this case, free space occupies the "reciprocity volume" for both the asymptotic and test cases -- the conducting cylinder falls outside that volume. Figure 20 illustrates the preceding discussion. Since the planar image of the test source falls inside the mathematical surface

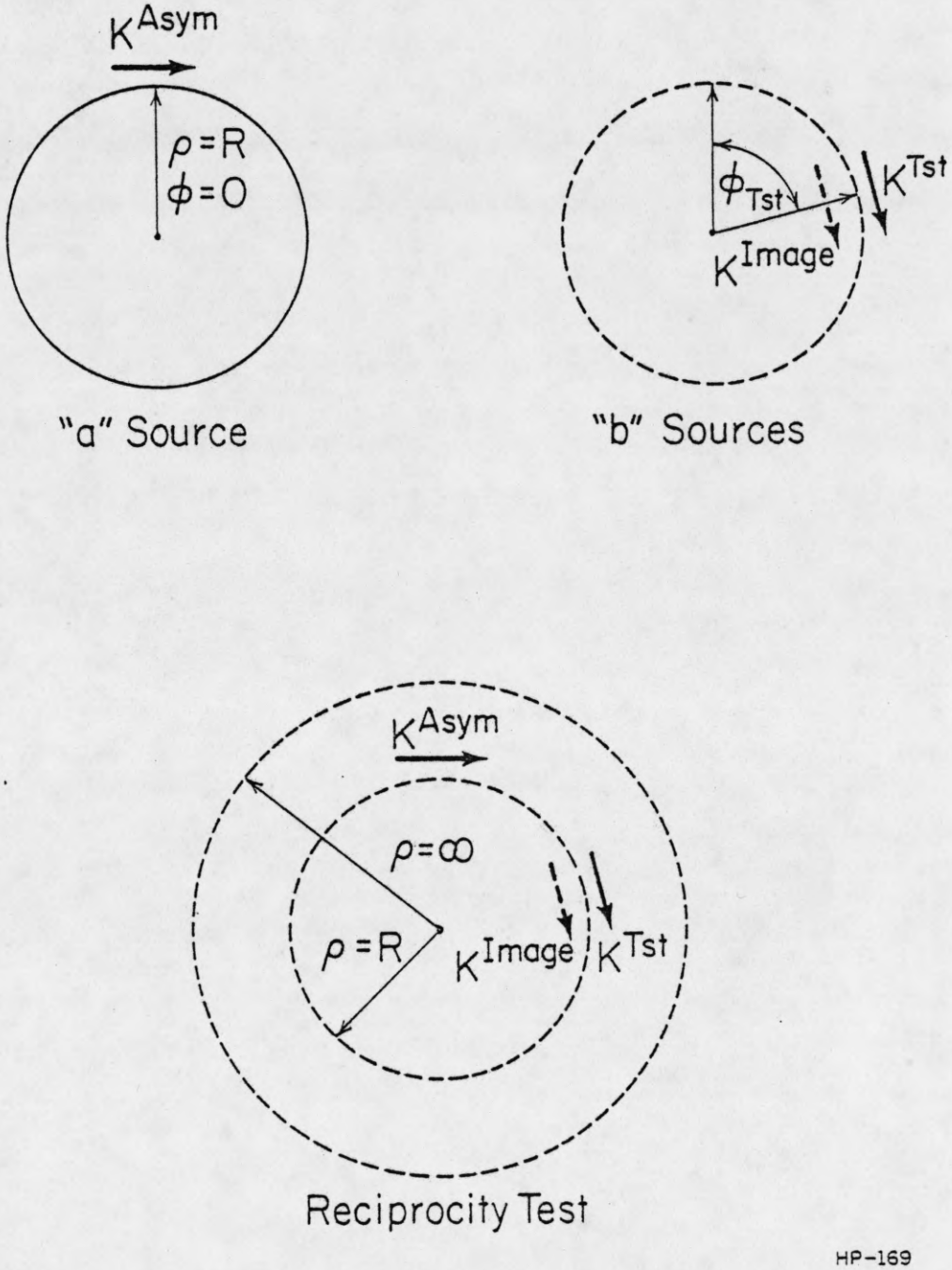

Fig. 20. Formulation of Reciprocity Test.

defining the cylinder, only the asymptotic source and the test source (not its image) fall inside the reciprocity volume. The asymptotic source is of the form $\delta(\rho-(R+\Delta))\delta(\phi)\delta(z)$ and the test source has the form $\delta(\rho-(R+\Delta))\delta(\phi-\phi_{TST})\delta(z-z_{TST})$, where Δ is the distance of the dipoles above the cylinder surface. The reciprocity equation reduces to (Eq. 3.0-3)

$$-\oint_S \left(\bar{E}^{ASY} \times \bar{H}^{TST} - \bar{E}^{TST} \times \bar{H}^{ASY} \right) \cdot d\bar{s} = \bar{H}^{ASY}\Big|_{\substack{\rho=R+\Delta \\ \phi=0 \\ z=0}} - \bar{H}^{TST}\Big|_{\substack{\rho=R+\Delta \\ \phi=\phi_{TST} \\ z=z_{TST}}}$$

Δ will be taken to be vanishingly small, so the surface fields are used in evaluation of the right-hand $\bar{H}^{ASY}$ term. We know that if the asymptotic source dipole is raised above the surface, then the surface E-fields should be zero everywhere on the cylinder surface. The reciprocity surface is vanishingly close to the cylinder surface so the true solution should satisfy (Eq. 3.0-4)

$$0=\oint_S \bar{E}^{ASY} \times \bar{H}^{TST} \cdot d\bar{s} = \oint_S \bar{E}^{TST} \times \bar{H}^{ASY} \cdot d\bar{s} + \bar{H}^{ASY}\Big|_{TST} - \bar{H}^{TST}\Big|_{ASY}$$

It is this equation that defines the reciprocity test, <u>i.e.</u>, the reciprocity test consists of checking to see how closely the asymptotic solutions satisfy (3.0-5)

$$\oint_S \bar{E}^{TST} \times \bar{H}^{ASY} \cdot \hat{n}\, ds + \bar{H}^{ASY}\Big|_{TST} - \bar{H}^{TST}\Big|_{ASY} = 0$$

where the surface S is the cylinder surface, and $\hat{n}$ is defined as $\hat{n}=(-\hat{\rho})$. For all work reported here, the asymptotic source dipole was defined as $\bar{K}^{ASY} = \delta(\rho-R)\delta(\phi)\delta(z)$ and the test dipole as $\bar{K}^{TST}=\delta(\rho-R)\,\delta(\phi)\,\delta(z-z_{TST})$; that is, both lie on the cylinder surface

along the ϕ=0 cut. The test equation can then be expanded to

$$\oint_{CYL}(E_z^{TST}H_\phi^{ASY} - E_\phi^{TST}H_z^{ASY})\,ds + H_\phi^{ASY}\Big|_{\substack{\rho=R\\ \phi=0\\ z=z_{TST}}} - H^{TST}\Big|_{\substack{\rho=R\\ \phi=0\\ z=0}} = 0, \qquad \text{(Eq. 3.0-6)}$$

and again the test fields are those from a magnetic dipole and its planar image radiating in free space.

Observe that when both the test and asymptotic source dipoles are located along ϕ=0, then a very desirable event occurs. The most difficult and time-consuming part of the reciprocity test is, of course, evaluation of the surface integral; and the most difficult part of that evaluation would be in the source regions of the magnetic dipoles. When both sources lie along the same ϕ cut, however, the plane of zero tangential E-fields from the test source coincides with the location of the peaky source region behaviour of the asymptotic source. Thus, a zero or very small E-field value from the test source will cancel or reduce the large H-fields near the asymptotic source, making evaluation of the integral much easier. Convergence checks on the surface integral confirm that evaluation of the integral is quite straightforward, and it is not necessary to resort to any great subtleties to get an accurate computation. If the test source is located along a different ϕ-cut than the asymptotic source, then no cancellation occurs and it becomes necessary to derive other schemes to evaluate the integral. This subject will be discussed in a future work, but for this report, both source dipoles are located along ϕ=0 and the integral is calculated numerically.

3.1 Results of Reciprocity Test

The reciprocity test was applied to the OSU, OSUMOD, and UI solutions. The position of the test dipole was varied from z_{TST}=0.5 wavelength out to z_{TST}=8.0 wavelengths in half-wavelength steps. The cylinder radius was 1.517 wavelengths and the integral involved was calculated numerically. In evaluation of the integral the full 2π radian range of ϕ was sampled using 25 points per radian. Sampling in z was 10 points per wavelength, and the integral was sampled in z for an extent of z_{TST} plus three wavelengths. The sampling range in z (which extended for 1.5 wavelengths past each dipole source) was established during a check of convergence of the integral, when it was found that this sampling is sufficient.

Figure 21 presents results of the reciprocity test. If ε is defined as the error in the solution

$$\varepsilon = \oint_S \bar{E}^{TST} \times \bar{H}^{ASY} \cdot \hat{n}\, ds + \bar{H}^{ASY}\Big|_{TST} - \bar{H}^{TST}\Big|_{ASY}, \qquad \text{(Eq. 3.0-6)}$$

then the ordinate is ε normalized by the value the asumptotic solution predicted for the H-field, i.e., ε divided by $\bar{H}_{\phi}^{ASY}\Big|_{TST}$.

For near-in regions ($z_{TST} < 1.5\ \lambda$) the OSUMOD and UI solutions are quite close. This might be expected, since both have the same origin behaviour in the limit. The OSU solution, which does not have the $1/s^2$ and $1/s^3$ terms, shows a much larger relative error near the source. As the test dipole moves away from the source, the relative error of the OSUMOD solution increases until it matches that of the OSU solution at around four to four and one-half wavelengths. This can be thought of as defining the region that is affected by the lack of higher-order terms in the OSU solution. The large path length

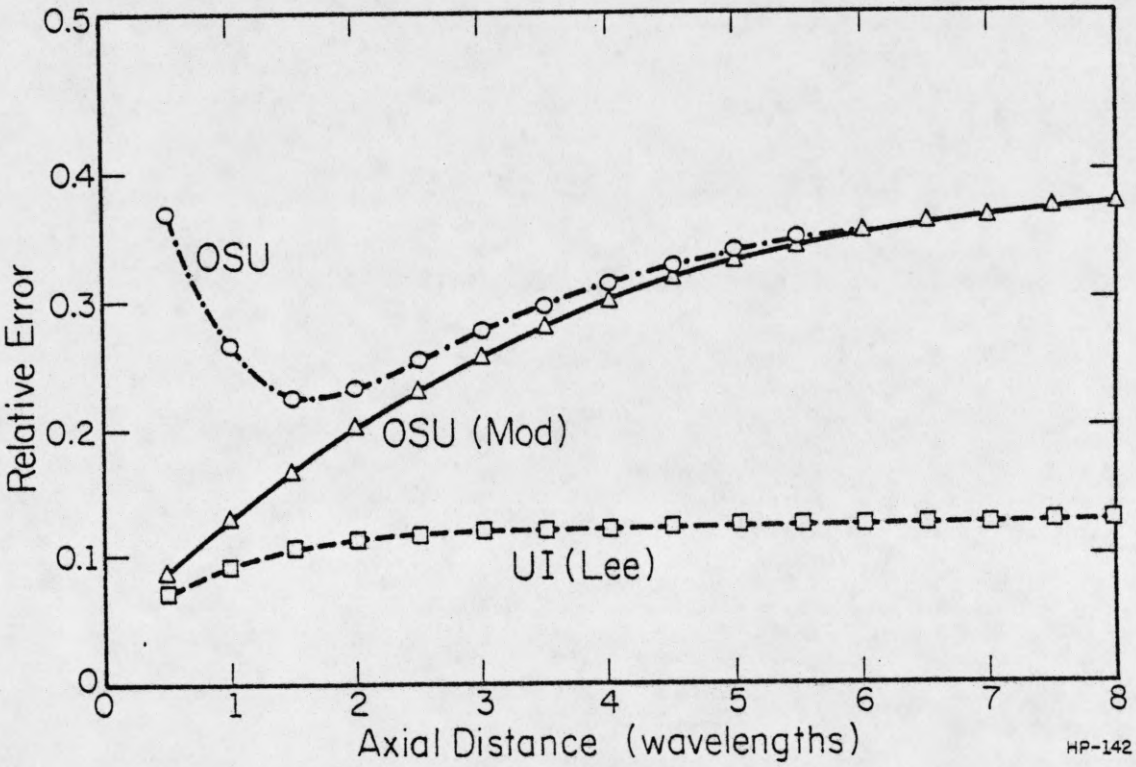

Fig. 21. Results of Reciprocity Test

behaviour of the OSU and OSUMOD solutions is practically identical, and this is reflected in the fact that the OSU and OSUMOD curves are indistinguishable for locations of the test dipole greater than five wavelengths away from the asymptotic source. While both the OSU and OSUMOD solutions show an increasing relative error as the separation increases, the relative error of the UI curve is nearly constant.

Since the normalizing value of $H_{\phi}^{ASY}\Big|_{TST}$ changes for each solution, one might argue that for identical ε values the "relative error" test is prejudiced against the OSU solution because it would always have a smaller denominator than the UI solution. For large path lengths, the OSU and OSUMOD solutions would appear to have larger relative error than the UI solution, because they decay as 1/s while UI decays as $1/\sqrt{s}$. This is certainly a valid comment, however, the actual results were:

$$\varepsilon_{OSU} > \varepsilon_{OSUMOD} \geq \varepsilon_{UI} \quad \text{source region test, and}$$

$$\varepsilon_{OSU} \geq \varepsilon_{OSUMOD} > \varepsilon_{UI} \quad \text{large path length test.}$$

The "relative error" presentation may tend to emphasize the differences, but it does not distort them, as can be seen in Table 1 which presents the unnormalized results.

Table 1

Unnormalized Results of Reciprocity Test

separation (λ)	ε_{OSU}	ε_{OSUMOD} (x 10**-4)	ε_{UI}
0.5	19.2	4.6	4.6
1.0	6.4	3.5	2.8
1.5	4.0	2.9	2.1
2.0	3.0	2.5	1.7
2.5	2.5	2.3	1.5
3.0	2.3	2.1	1.3
3.5	2.0	2.0	1.2
4.0	1.8	1.8	1.1
4.5	1.7	1.6	1.0
5.0	1.6	1.6	0.94
6.0	1.4	1.4	0.85
7.0	1.3	1.3	0.75
8.0	1.3	1.3	0.67

3.2 Iterative Equation from Reciprocity Test

The exact solution to the cylinder problem would satisfy the equation

$$\varepsilon = 0 = \oint_s \overline{E}^{TST} \times \overline{H}^{EXACT} \cdot \hat{n}\, ds + \overline{H}^{EXACT}_{\phi}\Big|_{TST} - \overline{H}^{TST}\Big|_{EXACT}.$$

If $\overline{H}^{EXACT}$ is replaced by $\overline{H}^{ASY}$ for the asymptotic solution under test, one can observe that $\overline{H}^{ASY}$ occurs twice in the equation and once as an isolated value at a point. This suggests an iterative equation of the form

$$\overline{H}^{ASY}\Big|^{(1)}_{TST} = \overline{H}^{TST}\Big|_{ASY} - \oint_s \overline{E}^{TST} \times \overline{H}^{ASY}(\alpha) \cdot \hat{n}\, ds \qquad \text{(Eq. 3.2-1)}$$

where the asymptotic H-field is used to evaluate the integral, and that result is then used to update the value of the H-field on the cylinder. This has been applied to the points tested (from 0.5 to 8.0 wavelengths along ϕ=0) for the OSU and UI solutions. Table 2 presents the zeroth and iterated first-order results that are shown graphically in Figure 22.

Table 2. Results of Iterative Equation

H_ϕ AFTER FIRST ITERATION ($|| \times 10^{-4}$)

SEPARATION (λ)	ZERO ORDER		FIRST ORDER	
	OSU	LEE	OSU	LEE
4.5λ	5.894 89.8°	8.419 73.3°	7.22 80.1°	7.438 75.2°
5.0λ	5.304 -90.1°	7.706 -107.1°	6.577 -100.0°	6.798 -105.2°
5.5λ	4.822 89.9°	7.117 72.6°	6.036 88.9°	6.26 74.5°
6.0λ	4.421 -90.1°	6.622 -107.8°	5.575 -100.2°	5.797 -105.9°
7.0λ	3.789 -90.1°	5.836 -108.5°	4.875 -100.7°	5.101 -107.0°
8.0λ	3.316 -90.1°	5.239 -109.1°	4.351 -100.7°	4.579 -107.5°

RECIPROCITY TEST

$$0 = H_\phi^A|_B - H_\phi^B|_A$$

$$+ \oint\!\!\oint (E_Z^B H_\phi^A - E_\phi^B H_Z^A)\, ds$$

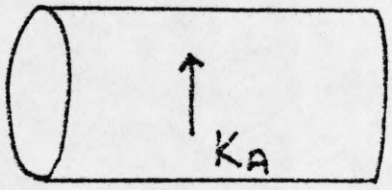

ITERATION

$$H_\phi^{A,(1)} = H^B - \oint\!\!\oint (E^B H^{A,(0)})\, ds$$

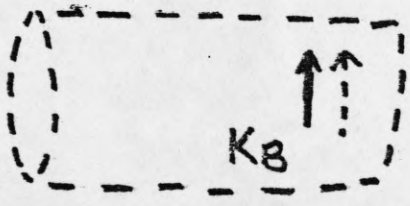

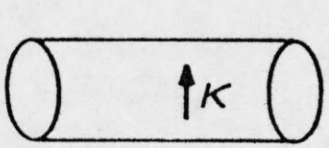

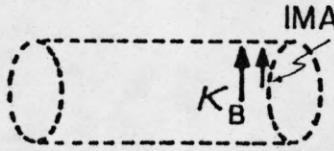

$$-H_\phi^A\Big|_B + H_\phi^B\Big|_A = \int_S (E_z^B H_\phi^A - E_\phi^B H_z^A)\, ds$$

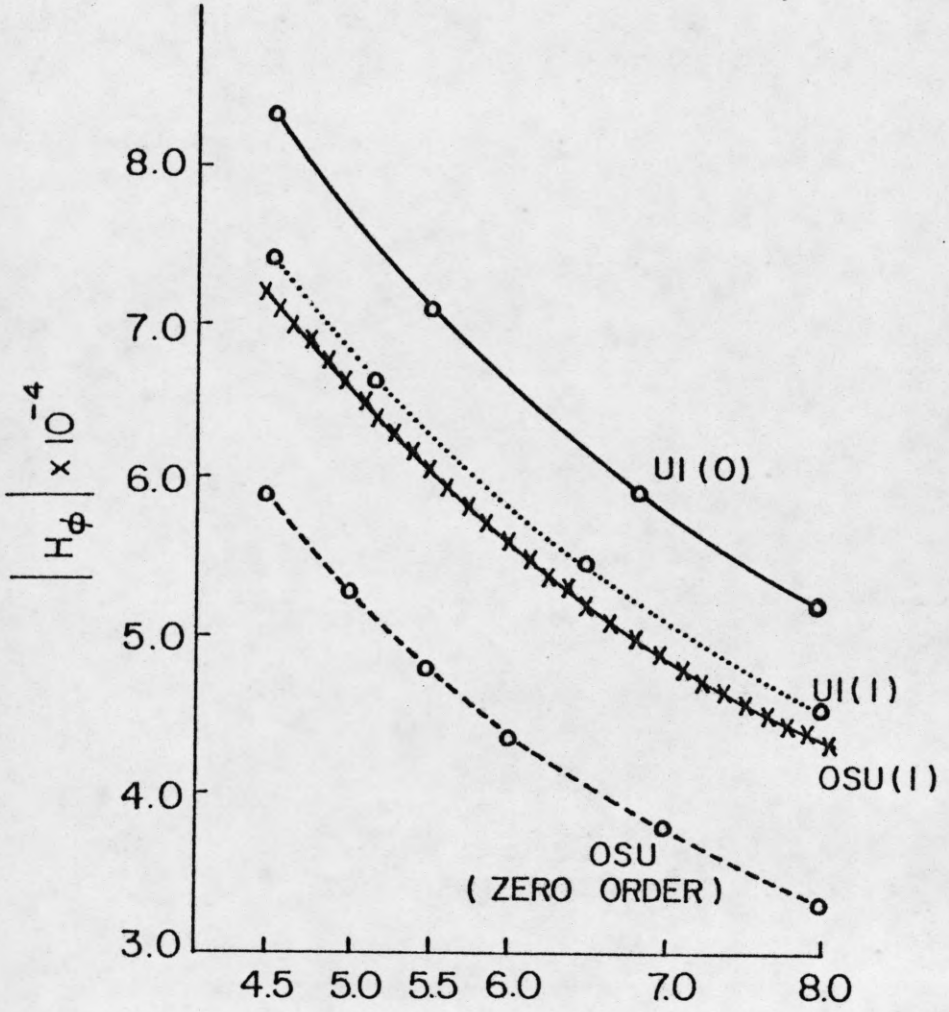

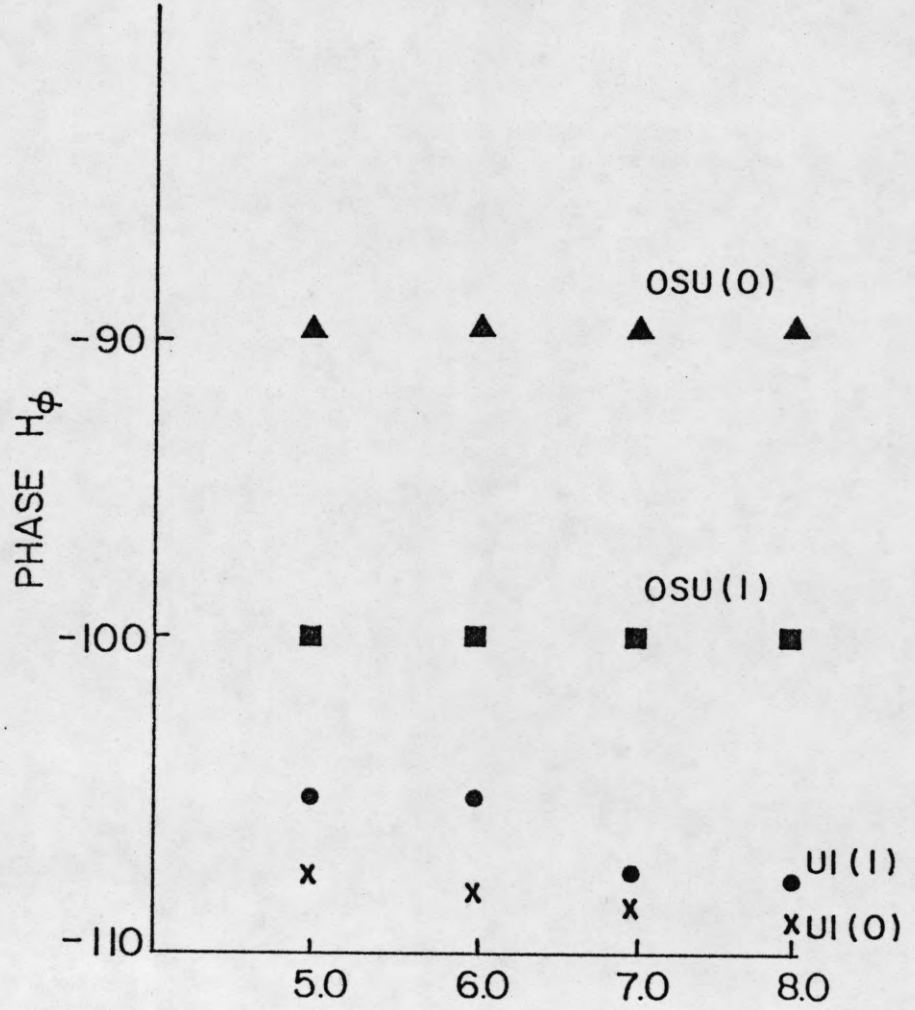

AXIAL SEPARATION – λ

Fig. 22. Results of Iterative Equation

The iterated magnitudes of the OSU solution uniformly increase, while the iterated magnitudes of the UI solution uniformly decrease. A similar result can be seen for the phase angle. The overall result is that in both magnitude and phase the iterated $UI^{(1)}$ and $OSU^{(1)}$ values are much closer than the zeroth-order solutions. This would appear to indicate that repeated application of the iterative equation can yield a better solution than either asymptotic solution alone.

3.3 Discussion of the Reciprocity Test

A prime objective in pursuing the reciprocity test was the attainment of a check that would reveal some features about the local accuracy of an asymptotic solution. The preliminary results of a check along only one ϕ cut are quite encouraging in that regard. In the source region, where the OSUMOD and UI solutions have a similar character, the test results are quite close. Both the OSUMOD and UI solutions show better test results near the source region than the OSU solution, which lacks the higher order terms present in the planar case. For large path lengths where the OSU and OSUMOD solutions agree, their test results are very close. The UI solution shows much less relative error for large path lengths than either the OSU or OSUMOD solutions, perhaps indicating that a $1/\sqrt{s}$ decay is closer to the true behaviour than a $1/s$ decay. Overall, the reciprocity test seems to offer great promise for providing a test which can evaluate the local accuracy of a solution.

4.0 Conclusions

Two tests have been proposed for evaluating the accuracy of asymptotic solutions to the problem of radiation from an infinite circular cylinder. The "E-Field Test" is based on satisfaction of the E-field boundary condition. This form of test is well-known, and has been applied to the solution of wire antennas by moment methods [8], and to asymptotic solutions of scattering problems [9],[10]. This work, however, presents the initial application of such a test to asymptotic solutions to the radiation problem. The "Lorentz Reciprocity Test" involves introduction of auxiliary sources and a check of how well the asymptotic solution satisfies Lorentz reciprocity. It is believed that this is the first time Lorentz reciprocity has been so employed.

The E-field test was applied to three different asymptotic solutions. The source region character of the radiation problem introduced computational difficulties; however, these were circumvented by use of a hybrid computation (as opposed to direct computation via an FFT). It was found that the E-field test was most sensitive to the behaviour of the solution in the source region, and relatively insensitive to the solution's large path length behaviour. That is, solutions whose source region had the form of the canonic planar solution as the radius increased showed a better E-field test than a solution which lacked the higher-order ($1/s^2$, $1/s^3$) terms present in radiation from a plane. In contrast, solutions with the same source region behaviour but different large path length behaviour showed inconsequential differences in satisfying the E-field boundary

condition.

The reciprocity test had a point-test character because a test source was employed. That is, preliminary results indicate that the local accuracy of a solution can be tested somewhat independently of the rest of the solution; i.e., each test can be associated with the result of an asymptotic solution at a specific point on the cylinder. The reciprocity test was used to check the three asymptotic solutions at points along the same ϕ-cut as the source ("propagation" along the cylinder axis with no phi-directed propagation). For close-in points the reciprocity test confirmed the E-field test results indicating the importance of the higher-order source-region terms. More importantly, the reciprocity test does differentiate between solutions with the same source-region behaviour and different large path length behaviour. In this case, a solution that showed attenuation of the form $1/\sqrt{s}$ satisfied the reciprocity test better than a solution which attenuated as $1/s$, for a large separation between the source and test points.

An iterative equation was achieved from the reciprocity test. Application to the tested points showed that the iterated, first-order results were much closer than the original, zeroth-order values for two asymptotic solutions.

The two tests presented are complementary. The E-field test is global in nature, and provides information about the source region accuracy (which affects most the self-impedance and near-in mutual-impedance terms). The Lorentz Reciprocity test has a discrete character and can provide information about the long path length

accuracy of a solution. In the regions where both tests apply, the two tests confirm one another.

Future work will be concerned with applying the reciprocity test to angles other than on-axis. The iterative equation from the reciprocity test could be employed to build up a complete first-order iterated solution. Finally, the reciprocity test might be used to check the exact modal solution, providing a means of confirming the validity of the test. The extension of the tests to axial slots does not appear to create any new problems.

5.0 References

[1] L. L. Bailin, "The Radiation Field Produced by a Slot in a Large Circular Cylinder," IRE Trans., vol. AP-3, no. 3, pp. 128-137, July, 1955.

[2] R. F. Harrington, Time-Harmonic Electromagnetic Fields. New York: McGraw-Hill Book Company, 1961.

[3] Y. Hwang and R. G. Kouyoumjian, "The mutual coupling between slots on an arbitrary convex cylinder," ElectroScience Laboratory, Department of Electrical Engineering, The Ohio State University, Semi-Annual Report 2902-21, prepared under Grant NGL 36-003-138, 1975.

[4] P. H. Pathak, "Analysis of a conformal receiving array of slots in a perfectly-conducting circular cylinder by the geometrical theory of diffraction," ElectroScience Laboratory, Department of Electrical Engineering, The Ohio State University, Technical Report ESL 3735-2, prepared under Contract N00140-74-C-6017, 1975.

[5] Z. W. Chang, L. B. Felsen, A. Hessel and J. Shmoys, "Surface ray method in the analysis of conformal arrays," Digest of 1976 AP-S International Symposium, held at the University of Massachusetts at Amherst, October 1976, pp. 366-369.

[6] Z. W. Chang, L. B. Felsen, and A. Hessel, "Surface ray methods for mutual coupling in conformal arrays on cylinder and conical surface," Polytechnic Institute of New York, Final Report (September 1975-February 1976), prepared under Contract N00123-76-C-0236, 1976.

[7] S. W. Lee and S. Safavi-Naini, "Asymptotic Solution of Surface Field due to a Magnetic Dipole on a Cylinder," Electromagnetics Laboratory, Department of Electrical Engineering, University of Illinois at Urbana-Champaign, Technical Report No. 76-11, supported by Contract N00019-76-M-0622, 1976.

[8] E. K. Miller and F. J. Deadrick, "Some Computational Aspects of Thin-Wire Modeling," in Topics in Applied Physics, R. Mittra, Ed. New York: Springer-Verlag, 1975.

[9] W. L. Ko and R. Mittra, "A New Approach Based on a Combination of Integral Equation and Asymptotic Techniques for Solving Electromagnetic Scattering Problems," IEEE Trans. Antennas and Propogation, vol. AP-25, no. 2, pp. 187-197, 1977.

[10] R. Mittra, Y. Rahmat-Samii, and W. L. Ko, "Spectral Theory of Diffraction," Appl. Physics, vol. 10, pp. 1-13, 1976.